Diamond & Related Materials 136 (2023) 109993

Contents lists available at ScienceDirect

Diamond & Related Materials

journal homepage: www.elsevier.com/locate/diamond

Acoustoelectric direct current density in fluorine doped single-walled carbon nanotubes due to harmonic mixing of bichromatic fields with commensurate frequencies

D. Sekyi-Arthur Dr, Ph.D [a,*], S.Y. Mensah Dr, Ph.D [b], E.K. Amewode Dr, Ph.D [b], R. Arthur Mr., MPhil [c], R.R. Adams Miss, MPhil [d]

[a] Department of Physics, School of Physical and Mathematical Sciences, University of Ghana, Legon, Ghana
[b] Department of Physics, College of Agriculture and Natural Sciences, U.C.C, Ghana
[c] Department of Physics Education, University of Education, PMB, Winneba, Ghana
[d] Department of Chemistry Education, College of Education, University of Cape Coast, PMB, Cape Coast, Ghana

ARTICLE INFO

Keywords:
Fluorine
Carbon nanotube
Semiconductor
Acoustoelectric
Bichromatic

ABSTRACT

Herein, we theoretically report on the acoustoelectric direct current (ADC) generation in a non-degenerate fluorine doped single-walled carbon nanotubes (FSWCNTs), due to mixing of waves with commensurate harmonics in the hypersound regime, $q\ell \gg 1$ (where q is the acoustic wavenumber and ℓ is the carrier mean free path). The only restriction of the theory on the sound intensity was that, the interaction energy between the carrier and the acoustic phonons must be small in comparison with the characteristic carrier energy. It was observed that in this situation, the higher harmonics of the effective field of the acoustic wave can be neglected; the origin of the nonlinearity was due to the distortion of the distribution function for carriers moving in phase with the phonons, as a result of interaction with the acoustic wave; the nonlinear effects can then be very important. The ADC generated was highly nonlinear and non-ohmic and depended on the amplitude of the bichromatic fields (i.e., pump and probe field), overlapping integral for jumps (Δ_s and Δ_z), carrier concentration (n_o), Bloch frequency (Ω), photon frequency (ω) and acoustic phonon frequency (ω_q). The strong nonlinearity and non-ohmicity of the I-V characteristic of the FSWCNTs may be associated with a number of nonlinear phenomena including the non-parabolic band relation, carrier heating due to distortion in carrier distribution function, Stark component, and Bloch oscillations of intraminiband carriers. It was possible to alter the magnitude and direction of the rectified ADC by adjusting the phase of the fields, and the generation of ADC corresponded to even instability zones in the FSWCNTs. Thus, based on the high ADC obtained, we propose FSWCNTs for ADC generation under bichromatic fields with commensurate harmonics.

1. Introduction

Coherent mixing of electromagnetic waves with comparable or commensurate (i.e. usually multiple) frequencies has been recognised to cause a dc generation phenomenon in a number of superconducting devices since the 1960s [1,2]. The origin of this phenomenon is the emergence of a variety of nonlinearities in semiconductors, mostly due to charge carrier heating as a result of the distortion in the carrier distribution function [2], and non-parabolicity of the conduction band [3]. Direct current generation effect in such structures may be reliably observed by utilising a medium which may ensure this, preferably a strong nonlinear semiconducting novel structure with non-parabolic dispersion relation [4,5].

However, even with parametric resonance, dc generation would not be possible if the system have complete spatial and temporal chronological symmetry. The absence of a microscopic centre of inversion in the system causes the dc generation effect (i.e., the ratchet effect) [6]. An ideal superstructure has a symmetric structure with an inversion center, so that the appearance of dc in such a system must be related to the breakdown of the temporal symmetry of the form; $\mathscr{E}(t) = -\mathscr{E}(t+$

* Corresponding author.
E-mail addresses: dsekyi-arthur@ug.edu.gh (D. Sekyi-Arthur), profsymensah@gmail.com (S.Y. Mensah), emmanuel.amewode@ucc.edu.gh (E.K. Amewode), bobarth28@yahoo.co.uk (R. Arthur), reginarakiaadams@gmail.com (R.R. Adams).

https://doi.org/10.1016/j.diamond.2023.109993
Received 1 February 2023; Received in revised form 2 May 2023; Accepted 3 May 2023
Available online 16 May 2023

$T/2$) (where $\mathscr{E}$ is the electric field strength and T is the common period of the fields being mixed). It is noteworthy that, only specific frequencies of mixed field ratios cause the temporal symmetry to be violated [7].

It is well known that system's instability leads to parametric resonance, and these parametric oscillations are triggered by an initial pulse (or initial fluctuation). Even if we assume that the system is an ideal one with symmetric structure from a theoretical standpoint, it is still impossible to anticipate these instabilities because the rectified current's direction is determined by random variables [7]. It is also noteworthy that, dc generation effect in bulk semiconductors is largely observed during the mixing of microwave radiation harmonics, even if mixing of terahertz waves is of greatest consequence for semiconductors. Because it directly links to the urgent modern scientific and technical concerns of terahertz radiation detection, generation, and amplification [7–9], the terahertz rectification effect in novel structures is very significant.

One of the most promising and actively researched methods for using structures such as superlattices (SLs) as the working medium of a compact terahertz radiation amplifier operating at room temperature of field frequency that is both similar to and dissimilar to the pump, is the use of a strong microwave pump (including polychromatic) field acting on the superlattice and amplifying the probe field [10–20]. The presence of a constant field component in this instance complements the parametric influence of the pump field's amplification of even harmonics (commensurate frequencies are those whose ratio can be stated by an irreducible rational fraction). The ability of an electromagnetic wave mixed with its second harmonic to be rectified in a SL was first demonstrated theoretically [7,10,16–20].

1-D nanostructures like single-walled carbon nanotubes (SWCNTs) have received a lot of attention due to their excellent electrical and thermal conductivities [21]. Multiple foreign atoms can bind to the surface of the SWCNTs thanks to their skeletal structure without endangering the tubular structure. An armchair-SWCNT can be made semiconducting by doping with fluorine atoms [21–28].

In this study, we assess the electromagnetic wave rectification capability of fluorine-doped SWCNTs and the carrier momenta in the presence of acoustic phonons (FSWCNT). The geometric chiral angle (GCA, θ_h), temperature (T), and the real overlapping integrals for leaps along the tubular axis (Δ_z) and base helix (Δ_s), respectively, all play a significant role in the aforementioned properties [21,26–28]. FSWCNT is a possible competitor for terahertz applications because it can produce an acoustoelectric direct current density when these parameters vary. As far as we know, no studies have looked at the ADC density of FSWCNTs under bichromatic fields with comparable frequencies. The purpose of this study was to look at the non-parabolic double periodic band of FSWCNT's acoustoelectric current density.

2. Theory

The problem is solved with the following quasi-classical conditions: (i) $\Delta_{s,z} \gg \tau^{-1} (\hbar = 1)$, (ii) $\omega \gg 1/\tau$; (iii) $\omega_q \ll \varepsilon(p)$; (iv) $\omega \gg \Delta_{s,z}$; (v) carriers are available only in the lowest miniband and interminiband transitions are neglected; (vi) carrier gas was nondegenerate; (vii) phonons are in the state of thermal equilibrium; where the externally applied bichromatic electric field, is directed along the FSWCNT axis; (viii) For a frequency range of 100GHz to 3THz and a nanotube of 100 nm at a high temperature $> 50K$ (or 5 meV), low temperature quantum effects such as Coulomb blockade etc. becomes non-significant. This approach becomes valid as soon as any electric field characteristic with the dimensions of "frequency" (a.c. field frequency, Stark frequencies corresponding to dc and ac field intensities) is less than the overlapping integral [29].

(ix) For hypersound regime $q\ell \gg 1$ and $\omega\tau \gg 1$, wave phenomena such as reflection and tunneling are absent and so the high frequency phonons are considered as particles with energy and momentum and thus, can be treated semiclassically. For slowly varying potentials (where carrier energy is assumed to be greater than the potential energy), reflections do not occur. The absence of reflection can be understood only if the slowly varying potential is approximated by a large number of small potentials. The small reflections that occur at each interface add destructively so that no net reflections occur. Carrier motion in a slowly varying potential in this case, can be described semiclassically because reflections do not occur and the carriers obeys Newton's law.

(x) If the overlapping integral is greater than the energy picked up by the carrier from the external electric $(i.e. \Delta_{s,z} \gg eEd_{s,z})$ along the characteristic length of the FSWCNT and the scattering rate ν is small $h\nu < eEd_{s,z}$, then the carrier oscillate inside the first miniband with a so-called Bloch frequency $\Omega = eEd_{s,z}/\hbar$. The quasi-particle energy ($\varepsilon(p)$) and quasi-particle group velocity ($v = \partial\varepsilon(p)/\partial p$) along the FSWCNT axes are periodic function of time. Thus, we assume that the semi-classical condition; $\Delta_{s,z} \gg eEd_{s,z}$ is fulfilled. Once this requirement is satisfied, the conduction electron can be treated semi-classically, i.e., described by classical equations of motion, by the classical kinetic equation, etc., while bearing in mind that the carrier energy is a rather intricate function of the quasi-momentum because of the periodicity of the potential seen by the carrier.

(xi) In addition, the carrier wave packet is treated as a particle; the uncertainty in momentum is assumed to be minimal so that the carrier's energy is sharply defined, and the uncertainty in the carrier's position is assumed to be minimal compared to the distance over which the applied and built-in potentials significantly vary. The motion of the center of this wave packet is described by $\hbar dk/dt = -\nabla\varepsilon = F$ which looks like the classical relation between force and momentum.

For doped-SWCNTs (FSWCNTs), the relaxation time $\tau(\tau = 10^{-11}s)$ is very small than in undoped SWCNTs. For an ultrasonic wave whose length $\lambda = 2\pi/q$, is much less than the carrier free path length ($\lambda = 10^{-8}cm$), $q\ell \gg 1$ is satified (where λ is the phonon wavelength and ℓ is the carrier mean free path ($\ell = 1\mu m$)).

Moreover, we considered the response of carriers, belonging to a single miniband of FSWCNT, where carriers with energies below the energy of the interband transitions move in the crystalline field like free quasi-particles, with a modified dispersion law which allowed us to apply a quasi-classical approach to describe the carrier motion. The bichromatic electric field is written as, $\mathscr{E} = [\mathscr{E}_o + \mathscr{E}_1 cos(\omega_1 t) + \mathscr{E}_2 cos(\omega_2 t + \varphi_o)]$. $\mathscr{E}_{pr} = \mathscr{E}_2 cos(\omega t + \varphi_o)$ is the weak signal (probe) field and $\mathscr{E}_p = \mathscr{E}_o + \mathscr{E}_1 cos(\omega_1 t)$ is the strong signal (pump field). We should note that in real devices, $\mathscr{E}_{pr}$ is a mode of the resonator tuned to a desirable terahertz frequency. It is note worthy that in the weak signal limit, which will be considered in detail below, the expression for the current contained only the relative phase of the fields; therefore, it is convenient to initially introduce the phase only for the probe field. We will also consider in this case the situation where ω_1 and ω_2 are commensurate (i.e., $\omega_1/\omega_2 = n/m$ where n and m are integers and n/m is irreducible fraction). In order to calculate the acoustoelectric current density, we invoke the expression [22–25]

$$J = \frac{e\Phi\Lambda^2 q^2 \tau}{\rho v_s \omega_q} \sum_p^{\infty} \int_0^{\infty} [f(p) - f(p+q)][v(p+q) - v(p)] \times \delta(\varepsilon_{p+q} - \varepsilon_p - \omega_q) dp. \quad (1')$$

Fig. 1a shows a one dimensional SWCNT doped with fluorine atoms. Considering a fluorine doped SWCNT (n, n) with the fluorine atoms forming a one-dimensional chain. A nanotube of this nature is equivalent to a band with unit cell as shown in Fig. 1b, where b is the bond length $(c - c)$. The width for the F-(n, n) tube equals n periods with a periodic length of $3b$, and the unit cell contains $N = 4n - 2$ carbon atoms and the atomic numbering in the unit cell of the F-(n, n) nanotube are shown in Fig. 1c. Doped SWCNTs have qualitatively new physical properties. For instance, dispersion laws are qualitatively different for doped and undoped SWCNTs. For an F-(5,5) nanotube, dispersion curves are as shown in Fig. 1d. In this case, the dispersion curve at the edge of

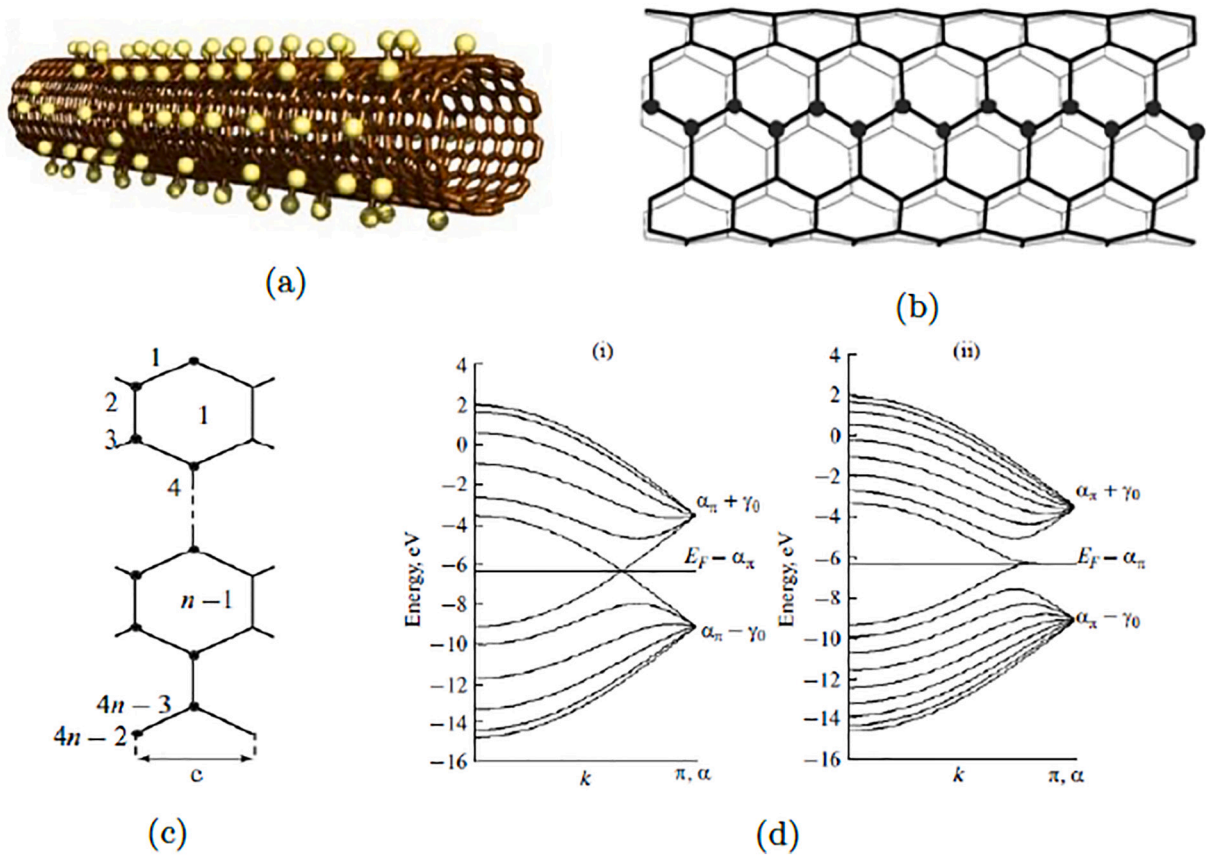

Fig. 1.. (a) Fluorine modified SWCNT with the fluorine atoms showing as yellow balls [25], (b) Fluorinated nanotube F − (n,n) (dots denotes the positions of Fluorine atoms of Fluorine atoms that are covalently bonded to C atoms) [30] (c) Atom numbering in the unit cells of nanotubes F − (n,n) [30] (d) $\pi-$ zone of (i) nanotube (5,5) (ii) nanotube F-(5,5), calculated with the parameters, $\alpha_\pi = -6.38$eV and $\beta_\pi = -2.79$eV found from benzene spectra [30].

the Brillouin zone lies on the Fermi surface and the derivative of this curve is zero.

For a conjugated $\pi-$ system in which there is alternation of single and double bonds along a linear chain, we used the Huckel matrix approximation to provide the energy dispersion relation for the FSWCNT as in Refs. [21,26–28]. The band relation for a $p-$ type band with periodicity $3b_{s,z}$ and two degree of freedom where the fluorine atoms form a one-dimensional chain was given as:

$$\varepsilon(p) = \varepsilon_o - \Delta_s cos\frac{p_s d_s}{\hbar} - \Delta_z cos\frac{p_z d_z}{\hbar}, \tag{2}$$

where $d_s = \sqrt{3}b_s/2$, $d_z = 3\sqrt{3}b_z/2$, and $b_{s,z}$ is the $c-c$ bond length along the helical and axial directions, respectively. The minimum energy of an outer-shell carrier in an isolated carbon atom is ε_o, and the real overlapping integral for leaps in the helical ($\mathscr{S}$) and axial ($\mathscr{Z}$) directions were Δ_s and Δ_z, respectively.

Proceeding as in Refs. [21,26–28], the carrier miniband velocity along the $\mathscr{S}$ and $\mathscr{Z}$ coordinates is calculated as followed:

$$v_s(p_s) = \frac{\Delta_s d_s}{\hbar} sin\left(\frac{p_s d_s}{\hbar}\right), \quad v_z(p_z) = \frac{\Delta_z d_z}{\hbar} sin\left(\frac{p_z d_z}{\hbar}\right). \tag{3}$$

In the presence of a high frequency bichromatic external electric field, the Boltzmann kinetic equation for carriers interacting with acoustic phonons of frequency (ω_q) and wavenumber (q) is quoted as:

$$\frac{\partial f(p,t)}{\partial t} + e[\mathscr{E}_o + \mathscr{E}_1 cos(\omega_1 t) + \mathscr{E}_2 cos(\omega_2 t + \varphi_o)]\frac{\partial f(p,t)}{\partial p} = -\frac{f(p,t) - f_o(p)}{\tau}, \tag{4}$$

where $f(p,t)$ denotes the non-equilibrium carrier distribution function, $f_o(p)$ denotes carrier equilibrium distribution function, $v(p)$ denotes carrier miniband velocity, $\mathscr{E}$ denotes external electric field, p denotes carrier quasi-momentum, and τ denotes carrier relaxation time. With initial conditions of $t' = t$ and $p' = p$, the equation of motion of the FSWCNT carriers in the presence of the external high-frequency bichromatic field is obtained as:

$$\frac{dp'}{dt'} = e[\mathscr{E}_o + \mathscr{E}_1 cos(\omega_1 t') + \mathscr{E}_2 cos(\omega_2 t' + \varphi_o)], \tag{5}$$

and the solution given as:

$$p' = e\mathscr{E}_o t' + \frac{e\mathscr{E}_1}{\omega_1}[sin(\omega_1 t') - sin[\omega_1(t - t')]] + \frac{e\mathscr{E}_2}{\omega_2}[sin(\omega_2 t' + \varphi_o) - sin[(\omega_2(t - t') + \varphi_o)]] \tag{6}$$

The solution to the BTE is derived by applying the transformation $p \rightarrow p - p'$ and making the assumption that τ is constant yields:

$$f(p,t)=\int_0^{\infty}\frac{dt'}{\tau}exp(-t'/\tau)f_o\left[p-\left(e\mathscr{E}_o t'+\frac{e\mathscr{E}_1}{\omega_1}[sin(\omega_1 t')-sin[\omega_1(t-t')]]\right.\right.$$
$$\left.\left.+\frac{e\mathscr{E}_2}{\omega_2}[sin(\omega_2 t'+\varphi_o)-sin[(\omega_2(t-t')+\varphi_o)]]\right)\right]. \tag{7}$$

The local equilibrium carrier distribution function is given by the shifted Fermi-Dirac function as:

$$f_o(p)=\frac{1}{1+exp\left[\left(\varepsilon(p_z)-\varrho\right)/kT\right]}, \tag{8}$$

$$f_o(p)=A^{\dagger}exp\left[\frac{\Delta_s}{\Theta}cos\left(\frac{p_s d_s}{\hbar}\right)+\frac{\Delta_z}{\Theta}cos\left(\frac{p_z d_z}{\hbar}\right)-\left(\frac{\varrho-\varepsilon_o}{\Theta}\right)\right]. \tag{10}$$

$A^{\dagger}$ was the normalisation constant determined to be [26–28]:

$$A^{\dagger}=\frac{n_o d_s d_z}{2I_o\left(\Delta_s^{*}\right)I_o\left(\Delta_z^{*}\right)}exp\left(\frac{\varrho-\varepsilon_o}{\Theta}\right), \tag{11}$$

where n_o is the carrier concentration, $I_n(x)$ is a modified Bessel function of order n, and k is Boltzmann's constant. Substituting Eqs. (7)–(11) into Eq. (1') yields:

$$J=\frac{e\Phi\Lambda^2q^2\tau A^{\dagger}}{\rho v_s\omega_q}\sum_p^{\infty}exp\left(\frac{\Delta_z}{\Theta}cos\left(\frac{p_z d_z}{\hbar}\right)\right)\int_0^{\infty}e^{-t'/\tau}\frac{dt'}{\tau}$$
$$\times\left[exp\left(\frac{\Delta_s}{\Theta}cos\left(p_s-e\mathscr{E}_o t'-\frac{e\mathscr{E}_1}{\omega_1}[sin(\omega_1 t')-sin[\omega_1(t-t')]]-\frac{e\mathscr{E}_2}{\omega_2}[sin(\omega_2 t'+\varphi_o)-sin[(\omega_2(t-t')+\varphi_o)]]\right)d_s\right)\right.$$
$$\left.-exp\left(\frac{\Delta_s}{\Theta}cos\left(p_s+q-e\mathscr{E}_o t'-\frac{e\mathscr{E}_1}{\omega_1}[sin(\omega_1 t')-sin[\omega_1(t-t')]]-\frac{e\mathscr{E}_2}{\omega_2}[sin(\omega_2 t'+\varphi_o)-sin[(\omega_2(t-t')+\varphi_o)]]\right)d_s\right)\right] \tag{12}$$
$$\cdot[v_s(p_s+q)-v_s(p_s)]\delta\left(\frac{\omega_q}{2\Delta_s sin\left(\frac{qd_s}{2}\right)}-sin\left(p_s+\frac{q}{2}\right)\right).$$

where T is the temperature, k is the Boltzmann's constant, $\mathscr{E}_o$, $\mathscr{E}_1$, $\mathscr{E}_2$ and ϱ denotes the static dc field, ac fields (pump and probe) and carriers' electrochemical potential, respectively.

Eq. (8) is changed into the Fermi-Dirac integral ($\mathscr{F}_{1/2}$) of order 1/2 when Eqs. (7) and (8) are substituted into Eq. (1'), as stated in Refs. [22–25,27,28]:

$$\mathscr{F}_{1/2}(\eta_f)=\frac{1}{\Gamma(1/2)}\int_0^{\infty}\frac{\eta_f^{1/2}d\eta}{1+exp(\eta-\eta_f)}, \tag{9}$$

Within the first Brillouin zone, we applied a transformation to change the summation over p into an integral over p as:

$$\sum_p^{\infty}\rightarrow\frac{2}{(2\pi\hbar)^2}\int_{-\pi/d_s}^{\pi/d_s}dp_s\int_{-\pi/d_z}^{\pi/d_z}dp_z,$$

and the acoustoelectric current density became

$$J=\frac{e\Phi\Lambda^2q^2\tau A^{\dagger}}{(2\pi\hbar)^2\rho v_s\omega_q}\int_{-\pi/d_z}^{\pi/d_z}exp\left(\frac{\Delta_z}{\Theta}cos\left(\frac{p_z d_z}{\hbar}\right)\right)dp_z\int_0^{\infty}e^{-t'/\tau}\frac{dt'}{\tau}$$
$$\times\left[exp\left(\frac{\Delta_s}{\Theta}cos\left(p_s-e\mathscr{E}_o t'-\frac{e\mathscr{E}_1}{\omega_1}[sin(\omega_1 t')-sin[\omega_1(t-t')]]-\frac{e\mathscr{E}_2}{\omega_2}[sin(\omega_2 t'+\varphi_o)-sin[(\omega_2(t-t')+\varphi_o)]]\right)d_s\right)\right.$$
$$\left.-exp\left(\frac{\Delta_s}{\Theta}cos\left(p_s+q-e\mathscr{E}_o t'-\frac{e\mathscr{E}_1}{\omega_1}[sin(\omega_1 t')-sin[\omega_1(t-t')]]-\frac{e\mathscr{E}_2}{\omega_2}[sin(\omega_2 t'+\varphi_o)-sin[(\omega_2(t-t')+\varphi_o)]]\right)d_s\right)\right] \tag{13}$$
$$\cdot[v_z(p_z+q)-v_z(p_z)]\delta\left(\frac{\omega_q}{2\Delta_s sin\left(\frac{qd_s}{2}\right)}-sin\left(p_s+\frac{q}{2}\right)\right).$$

where $(\varrho-\varepsilon_c)/kT\equiv\eta_f$. For a non-degenerate carrier gas, where the Fermi level is several kT below the conduction band edge ε_c, (i.e $kT\ll\varepsilon_c$), the integral in Eq. (9) modified to:

The carrier acoustoelectric current densities along the base helix ($\mathscr{S}$) and tubular ($\mathscr{Z}$) directions were obtained as [26–28]:
and

$$\mathscr{S} = -\frac{e\Phi\Lambda^2 q^2 \tau A^{\dagger}}{(2\pi\hbar)^2 \rho v_s \omega_q} \int_{-\pi/d_z}^{\pi/d_z} exp\left(\frac{\Delta_z}{\Theta} cos\left(\frac{p_z d_z}{\hbar}\right)\right) dp_z \int_0^{\infty} e^{-t'/\tau} \frac{dt'}{\tau}$$
$$\times \left[exp\left(\frac{\Delta_s}{\Theta} cos\left(p_s - e\mathscr{E}_o t' - \frac{e\mathscr{E}_1}{\omega_1}[sin(\omega_1 t') - sin[\omega_1(t-t')]] - \frac{e\mathscr{E}_2}{\omega_2}[sin(\omega_2 t' + \varphi_o) - sin[(\omega_2(t-t') + \varphi_o)]]\right) d_s\right)\right.$$
$$\left. - exp\left(\frac{\Delta_s}{\Theta} cos\left(p_s + q - e\mathscr{E}_o t' - \frac{e\mathscr{E}_1}{\omega_1}[sin(\omega_1 t') - sin[\omega_1(t-t')]] - \frac{e\mathscr{E}_2}{\omega_2}[sin(\omega_2 t' + \varphi_o) - sin[(\omega_2(t-t') + \varphi_o)]]\right) d_s\right)\right] \tag{14}$$
$$\cdot \left[v_z(p_z + q) - v_z(p_z)\right] \delta\left(\frac{\omega_q}{2\Delta_s sin\left(\frac{q d_s}{2}\right)} - sin\left(p_s + \frac{q}{2}\right)\right)$$

$$\mathscr{Z} = -\frac{e\Phi\Lambda^2 q^2 \tau A^{\dagger}}{(2\pi\hbar)^2 \rho v_s \omega_q} \int_{-\pi/d_s}^{\pi/d_s} exp\left(\frac{\Delta_s}{\Theta} cos\left(\frac{p_s d_s}{\hbar}\right)\right) dp_s \int_0^{\infty} e^{-t'/\tau} \frac{dt'}{\tau}$$
$$\times \left[exp\left(\frac{\Delta_s}{\Theta} cos\left(p_z - e\mathscr{E}_o t' - \frac{e\mathscr{E}_1}{\omega_1}[sin(\omega_1 t') - sin[\omega_1(t-t')]] - \frac{e\mathscr{E}_2}{\omega_2}[sin(\omega_2 t' + \varphi_o) - sin[(\omega_2(t-t') + \varphi_o)]]\right) d_z\right)\right.$$
$$\left. - exp\left(\frac{\Delta_s}{\Theta} cos\left(p_z + q - e\mathscr{E}_o t' - \frac{e\mathscr{E}_1}{\omega_1}[sin(\omega_1 t') - sin[\omega_1(t-t')]] - \frac{e\mathscr{E}_2}{\omega_2}[sin(\omega_2 t' + \varphi_o) - sin[(\omega_2(t-t') + \varphi_o)]]\right) d_z\right)\right] \tag{15}$$
$$\cdot \left[v_z(p_z + q) - v_z(p_z)\right] \delta\left(\frac{\omega_q}{2\Delta_z sin\left(\frac{q d_z}{2}\right)} - sin\left(p_z + \frac{q}{2}\right)\right).$$

In the presence of acoustic phonons, the carrier momenta along the base helix and tubular directions for the first and second quadrants of the first Brillouin zone are deduced as;

$$p_s^1 = \frac{1}{d_s} sin^{-1}\left(\frac{\omega_q}{2\Delta_s sin(q d_s/2)}\right) - \frac{q}{2} \quad p_s^2 = \frac{\pi}{d_s} sin^{-1}\left(\frac{\omega_q}{2\Delta_s sin(q d_s/2)}\right) - \frac{q}{2} \tag{16}$$

$$p_z^1 = \frac{1}{d_z} sin^{-1}\left(\frac{\omega_q}{2\Delta_z sin(q d_z/2)}\right) - \frac{q}{2} \quad p_z^2 = \frac{\pi}{d_z} sin^{-1}\left(\frac{\omega_q}{2\Delta_z sin(q d_z/2)}\right) - \frac{q}{2} \tag{17}$$

Substituting Eqs. (16) and (17) into Eq. (15) and invoking standard integrals, the acoustoelectric carrier current densities along the helical ($\mathscr{S}$) and tubular ($\mathscr{Z}$) directions yields:

$$\mathscr{S} = -\frac{e\Phi\Lambda^2 q^2 \tau n_o d_s^2 d_z \theta(1-\alpha_s^2)}{(\pi\hbar)^2 \rho v_s \omega_q \cdot \Delta_s sin(q d_s/2)\sqrt{1-\alpha_s^2 I_o(\Delta_s/\Theta)}}$$
$$\times \int_0^{\infty} e^{-t'/\tau} \frac{dt'}{\tau} \left[sinh\left(\frac{\Delta_s}{\Theta} sinAcosBsin\left(\frac{q d_s}{2}\right)\right) sinh\left(\frac{\Delta_s}{\Theta} cosAcosBcos\left(\frac{q d_s}{2}\right)\right)\right. \tag{18}$$
$$\left. - \frac{\Delta_s}{\Theta} cosAsinBsin\left(\frac{q d_s}{2}\right) cosh\left(\frac{\Delta_s}{\Theta} cosAcosBcos\left(\frac{q d_s}{2}\right)\right) cosh\left(\frac{\Delta_s}{\Theta} sinAcosBsin\left(\frac{q d_s}{2}\right)\right)\right],$$

and

$$\mathscr{Z} = -\frac{e\Phi\Lambda^2 q^2 \tau n_o d_s d_z^2 \theta(1-\alpha_z^2)}{(\pi\hbar)^2 \rho v_s \omega_q \cdot \Delta_z sin(q d_z/2)\sqrt{1-\alpha_z^2 I_o(\Delta_z/\Theta)}}$$
$$\times \int_0^{\infty} e^{-t'/\tau} \frac{dt'}{\tau} \left[sinh\left(\frac{\Delta_z}{\Theta} sinAcosBsin\left(\frac{q d_z}{2}\right)\right) sinh\left(\frac{\Delta_z}{\Theta} cosAcosBcos\left(\frac{q d_z}{2}\right)\right)\right. \tag{19}$$
$$\left. - \frac{\Delta_z}{\Theta} cosAsinBsin\left(\frac{q d_z}{2}\right) cosh\left(\frac{\Delta_z}{\Theta} cosAcosBcos\left(\frac{q d_z}{2}\right)\right) cosh\left(\frac{\Delta_z}{\Theta} sinAcosBsin\left(\frac{q d_z}{2}\right)\right)\right],$$

where θ, and Θ are the Heaviside step function, temperature in energy units, respectively. For $\Theta \gg \Delta_s$ and $\Theta \gg \omega_q$

$$\mathscr{S} = -\frac{e\Phi\Lambda^2 q^2 \tau n_o d_s^2 d_z \theta(1-\alpha_s^2)}{(\pi\hbar)^2 \rho v_s \omega_q \cdot \Delta_s sin(qd_s/2)\sqrt{1-\alpha_s^2} I_o(\Delta_s/\Theta)} \times \int_0^\infty e^{-t'/\tau}\frac{dt'}{\tau}\left[\left(\frac{\Delta_s}{\Theta}\right)^2 sinAcosAsin\left(\frac{qd_s}{2}\right)cos\left(\frac{qd_s}{2}\right)cosB^2 - \frac{\Delta_s}{\Theta}cosAsinBsin\left(\frac{qd_s}{2}\right)\right] \tag{20}$$

and

$$\mathscr{Z} = -\frac{e\Phi\Lambda^2 q^2 \tau n_o d_s d_z^2 \theta(1-\alpha_z^2)}{(\pi\hbar)^2 \rho v_s \omega_q \cdot \Delta_s sin(qd_z/2)\sqrt{1-\alpha_z^2} I_o(\Delta_z/\Theta)} \times \int_0^\infty e^{-t'/\tau}\frac{dt'}{\tau}\left[\left(\frac{\Delta_z}{\Theta}\right)^2 sinAcosAsin\left(\frac{qd_z}{2}\right)cos\left(\frac{qd_z}{2}\right)cosB^2 - \frac{\Delta_z}{\Theta}cosAsinBsin\left(\frac{qd_z}{2}\right)\right] \tag{21}$$

where

$$B = e\mathscr{E}_o d_{s,z} t' + \frac{e\mathscr{E}_1 d_{s,z}}{\omega_1}[sin(\omega_1 t') - sin[\omega_1(t-t')]] + \frac{e\mathscr{E}_2 d_{s,z}}{\omega_2}[sin(\omega_2 t' + \varphi_o) - sin[(\omega_2(t-t') + \varphi_o)]]. \tag{22}$$

Eqs. (20) and (21) reduced to

$$\mathscr{S} = J_{os}\int_0^\infty e^{-t'/\tau}\frac{dt'}{\tau}\left[cos^2 B - \frac{4\Theta cosAsin(qd_z/2)}{\Delta_s}sinB\right] \tag{23}$$

and

$$\mathscr{Z} = J_{oz}\int_0^\infty e^{-t'/\tau}\frac{dt'}{\tau}\left[cos^2 B - \frac{4\Theta cosAsin(qd_z/2)}{\Delta_z}sinB\right]. \tag{24}$$

Making use of the identity: $cos^2(x) = 1/2(1+cos(2x))$ yielded

$$\mathscr{S} = J_{os}\int_0^\infty e^{-t'/\tau}\frac{dt'}{\tau} \times \left[\frac{1}{2}\left(1 + e^{i2e\mathscr{E}_o d_s t'}\mathscr{R}e\left[e^{iz_1'(sin\omega_1 t - sin\omega_1(t-t'))+iz_2'(sin(\omega_2 t+\varphi_o)-sin(\omega_2(t-t'))+\varphi_o)}\right]\right) - \frac{4\Theta cosAsin(qd_s/2)}{\Delta_s}\mathscr{I}m\left[e^{iz(sin\omega_1 t - sin\omega_1(t-t'))+iz_2(sin(\omega_2 t+\varphi_o)-sin(\omega_2(t-t'))+\varphi_o)}\right]\right] \tag{25}$$

and

$$\mathscr{Z} = J_{oz}\int_0^\infty e^{-t'/\tau}\frac{dt'}{\tau} \times \left[\frac{1}{2}\left(1 + e^{i2e\mathscr{E}_o d_s t'}\mathscr{R}e\left[e^{iz'(sin\omega_1 t - sin\omega_1(t-t'))+iz_2'(sin(\omega_2 t+\varphi_o)-sin(\omega_2(t-t'))+\varphi_o)}\right]\right) - \frac{4\Theta cosAsin(qd_z/2)}{\Delta_z}\mathscr{I}m\left[e^{iz(sin\omega_1 t - sin\omega_1(t-t'))+iz_2(sin(\omega_2 t+\varphi_o)-sin(\omega_2(t-t'))+\varphi_o)}\right]\right] \tag{26}$$

The real part of Eq. (25) is expressed as;

$$\mathscr{S}_1 = J_{os}\int_0^\infty e^{-t'/\tau}\frac{dt'}{\tau}\left[\frac{1}{2}\left(1 + e^{i2e\mathscr{E}_o d_s t'}e^{iz_1' sin\omega_1 t}e^{-iz_1' sin\omega_1(t-t')} \times e^{iz_2' sin(\omega_2 t+\varphi_o)}e^{-iz_2' sin(\omega_2(t-t')+\varphi_o)}\right)\right] \tag{27}$$

Invoking the Jacobi-Anger expansion

$$exp(\pm ixsin\omega t) = \sum_{k=-\infty}^{\infty} J_k(x)exp(\pm ik\omega t)$$

Eq. (29) reduces to

$$\mathscr{S}_1 = \frac{J_{os}}{2}\int_0^\infty e^{-t'/\tau}\frac{dt'}{\tau}\left[\left(1 + e^{i2e\mathscr{E}_o d_s t'}\sum_{k_1=-\infty}\sum_{m_1=-\infty} J_{k_1}(z_1')J_{m_1}(z_1')e^{i(k_1-m_1)\omega_1 t}e^{im_1\omega_1 t'} \times \sum_{k_2=-\infty}\sum_{m_2=-\infty} J_{k_2}(z_2')J_{m_2}(z_2')e^{i(k_2-m_2)\omega_2 t}e^{im_2\omega_1 t'}e^{i(k_2-m_2)\varphi_o}\right)\right] \tag{28}$$

We let $k_i - m_i = \nu_i$ and solve Eq. (27) explicitly as

$$\mathscr{S}_1 = \frac{J_{os}}{2}\int_0^\infty e^{-t'/\tau}\frac{dt'}{\tau}\left[\left(1 + \sum_{k_1 k_2=-\infty}^{\infty}\sum_{\nu_1\nu_2=-\infty}^{\infty}\frac{J_{k_1}(z_1')J_{k_2}(z_2')J_{k_1-\nu_1}(z_1')J_{k_2-\nu_2}(z_2')}{\left[1+(2\Omega_o + k_1\omega_1 + k_2\omega_2)^2\tau^2\right]} \times exp(i\nu_2\varphi_o)exp(i[(\nu_1\omega_1 + \nu_2\omega_2)t])\right)\right] \tag{29}$$

Similarly, the imaginary part is obtained as

$$\mathscr{S}_2 = -\frac{J_{os}\Theta cosAsin(qd_s/2)}{\Delta_s sinAsin(qd_s)} \sum_{k_1k_2=-\infty}^{\infty} \sum_{\nu_1\nu_2=-\infty}^{\infty} J_{k_1}(z_1)J_{k_2}(z_2)J_{k_1-\nu_1}(z_1)J_{k_2-\nu_2}(z_2) \times \frac{[\Omega_o + k_1\omega_1 + k_2\omega_2]\tau exp(i\nu_2\varphi_o)exp(i[(\nu_1\omega_1 + \nu_2\omega_2)t])}{\left[1 + (\Omega_o + k_1\omega_1 + k_2\omega_2)^2\tau^2\right]} \tag{30}$$

We sum the real and imaginary part which yields

$$\mathscr{S} = \frac{J_{os}}{2}\left(1 + \sum_{k_1k_2=-\infty}^{\infty} \sum_{\nu_1\nu_2=-\infty}^{\infty} \frac{J_{k_1}(z_1')J_{k_2}(z_2')J_{k_1-\nu_1}(z_1')J_{k_2-\nu_2}(z_2')\langle cos[\nu_2\varphi_o + (\nu_1\omega_1 + \nu_2\omega_2)t]\rangle}{\left[1 + (2\Omega_o + k_1\omega_1 + k_2\omega_2)^2\tau^2\right]} - \frac{2\Theta cosAsin(qd_s/2)}{\Delta_s sinAsin(qd_s)} \sum_{k_1k_2=-\infty}^{\infty} \sum_{\nu_1\nu_2=-\infty}^{\infty} J_{k_1}(z_1)J_{k_2}(z_2)J_{k_1-\nu_1}(z_1)J_{k_2-\nu_2}(z_2) \times \frac{[\Omega_o + k_1\omega_1 + k_2\omega_2]\tau\langle sin[\nu_2\varphi_o + (\nu_1\omega_1 + \nu_2\omega_2)t]\rangle}{\left[1 + (\Omega_o + k_1\omega_1 + k_2\omega_2)^2\tau^2\right]}\right) \tag{31}$$

$$\mathscr{Z} = \frac{J_{oz}}{2}\left(1 + \sum_{k_1k_2=-\infty}^{\infty} \sum_{\nu_1\nu_2=-\infty}^{\infty} \frac{J_{k_1}(z_1')J_{k_2}(z_2')J_{k_1-\nu_1}(z_1')J_{k_2-\nu_2}(z_2')\langle cos[\nu_2\varphi_o + (\nu_1\omega_1 + \nu_2\omega_2)t]\rangle}{\left[1 + (2\Omega_o + k_1\omega_1 + k_2\omega_2)^2\tau^2\right]} - \frac{2\Theta cosAsin(qd_z/2)}{\Delta_z sinAsin(qd_z)} \sum_{k_1k_2=-\infty}^{\infty} \sum_{\nu_1\nu_2=-\infty}^{\infty} J_{k_1}(z_1)J_{k_2}(z_2)J_{k_1-\nu_1}(z_1)J_{k_2-\nu_2}(z_2) \times \frac{[\Omega_o + k_1\omega_1 + k_2\omega_2]\tau\langle sin[\nu_2\varphi_o + (\nu_1\omega_1 + \nu_2\omega_2)t]\rangle}{\left[1 + (\Omega_o + k_1\omega_1 + k_2\omega_2)^2\tau^2\right]}\right) \tag{32}$$

where

$$J_{os} = -\frac{e\Phi\Lambda^2q^2\tau n_o d_s^2 d_z\theta\left(1-\alpha_s^2\right)\Delta_s^2 sin(2A)sin(qd_s)}{4\Theta\pi\hbar^2\rho v_s\omega_q sin\left(\frac{qd_s}{2}\right)\sqrt{1-\alpha_s^2}I_o\left(\frac{\Delta_s}{\Theta}\right)} \tag{33}$$

$$J_{oz} = -\frac{e\Phi\Lambda^2q^2\tau n_o d_s d_z^2\theta\left(1-\alpha_z^2\right)\Delta_z^2 sin(2A)sin(qd_z)}{4\Theta\pi\hbar^2\rho v_s\omega_q sin\left(\frac{qd_z}{2}\right)\sqrt{1-\alpha_z^2}I_o\left(\frac{\Delta_z}{\Theta}\right)} \tag{34}$$

Without losing generality, we expressed the high frequency bichromatic acoustoelectric current density into axial and circumferential components as; $J_z = \overrightarrow{\mathscr{Z}}_q + \overrightarrow{\mathscr{S}}_q sin\theta_h$ and $J_s = \overrightarrow{\mathscr{S}}_q cos\theta_h$, respectively. The axial acoustoelectric current density is expressed as

$$J_z = \frac{J_{oz}}{2}\left(1 + \sum_{k_1k_2=-\infty}^{\infty} \sum_{\nu_1\nu_2=-\infty}^{\infty} \frac{J_{k_1}(z_1')J_{k_2}(z_2')J_{k_1-\nu_1}(z_1')J_{k_2-\nu_2}(z_2')\langle cos[\nu_2\varphi_o + (\nu_1\omega_1 + \nu_2\omega_2)t]\rangle}{\left[1 + (2\Omega_o + k_1\omega_1 + k_2\omega_2)^2\tau^2\right]} - \frac{2\Theta cosAsin(qd_z/2)}{\Delta_z sinAsin(qd_z)} \sum_{k_1k_2=-\infty}^{\infty} \sum_{\nu_1\nu_2=-\infty}^{\infty} J_{k_1}(z_1)J_{k_2}(z_2)J_{k_1-\nu_1}(z_1)J_{k_2-\nu_2}(z_2) \times \frac{[\Omega_o + k_1\omega_1 + k_2\omega_2]\tau\langle sin[\nu_2\varphi_o + (\nu_1\omega_1 + \nu_2\omega_2)t]\rangle}{\left[1 + (\Omega_o + k_1\omega_1 + k_2\omega_2)^2\tau^2\right]}\right) + \frac{J_{os}}{2}\left(1 + \sum_{k_1k_2=-\infty}^{\infty} \sum_{\nu_1\nu_2=-\infty}^{\infty} \frac{J_{k_1}(z_1')J_{k_2}(z_2')J_{k_1-\nu_1}(z_1')J_{k_2-\nu_2}(z_2')\langle cos[\nu_2\varphi_o + (\nu_1\omega_1 + \nu_2\omega_2)t]\rangle}{\left[1 + (2\Omega_o + k_1\omega_1 + k_2\omega_2)^2\tau^2\right]} - \frac{2\Theta cosAsin(qd_s/2)}{\Delta_s sinAsin(qd_s)} \sum_{k_1k_2=-\infty}^{\infty} \sum_{\nu_1\nu_2=-\infty}^{\infty} J_{k_1}(z_1)J_{k_2}(z_2)J_{k_1-\nu_1}(z_1)J_{k_2-\nu_2}(z_2) \times \frac{[\Omega_o + k_1\omega_1 + k_2\omega_2]\tau\langle sin[\nu_2\varphi_o + (\nu_1\omega_1 + \nu_2\omega_2)t]\rangle}{\left[1 + (\Omega_o + k_1\omega_1 + k_2\omega_2)^2\tau^2\right]}\right)sin^2\vartheta \tag{35}$$

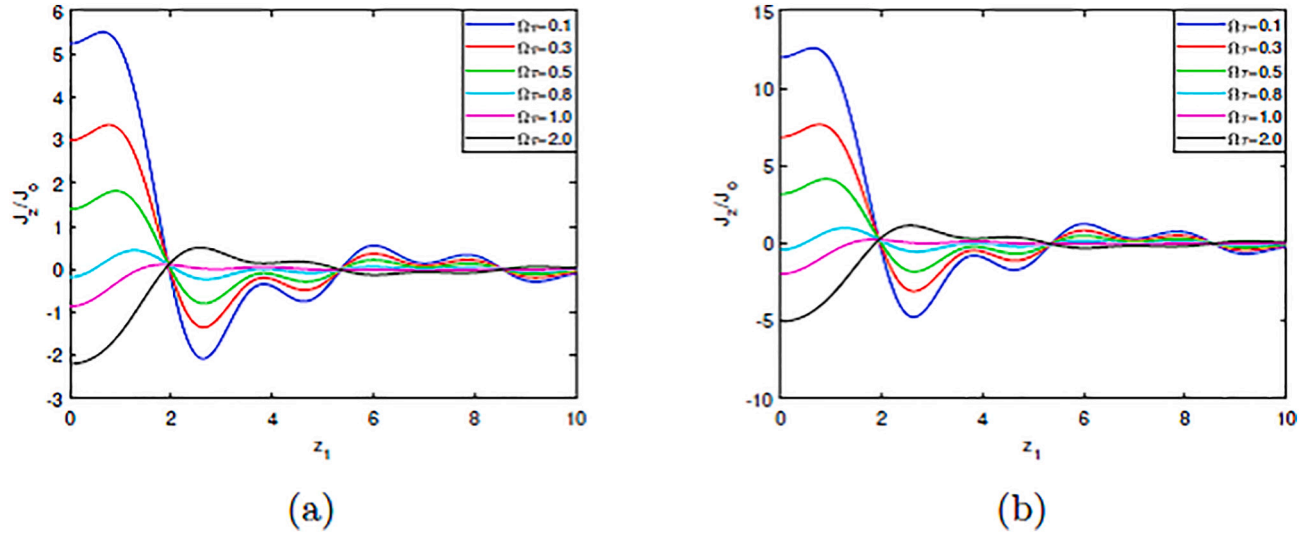

Fig. 2. Dependence of acoustocurrent (J_{zz}^{ae}/J_o^{ae}) on z_1 and z_2 for different values: (a) $\Omega\tau$, $\Delta_s = 0.25eV$ and $\Delta_z = 0.30eV$;(b) $\Omega\tau$, $\Delta_s = 0.30eV$ and $\Delta_z = 0.25eV$.

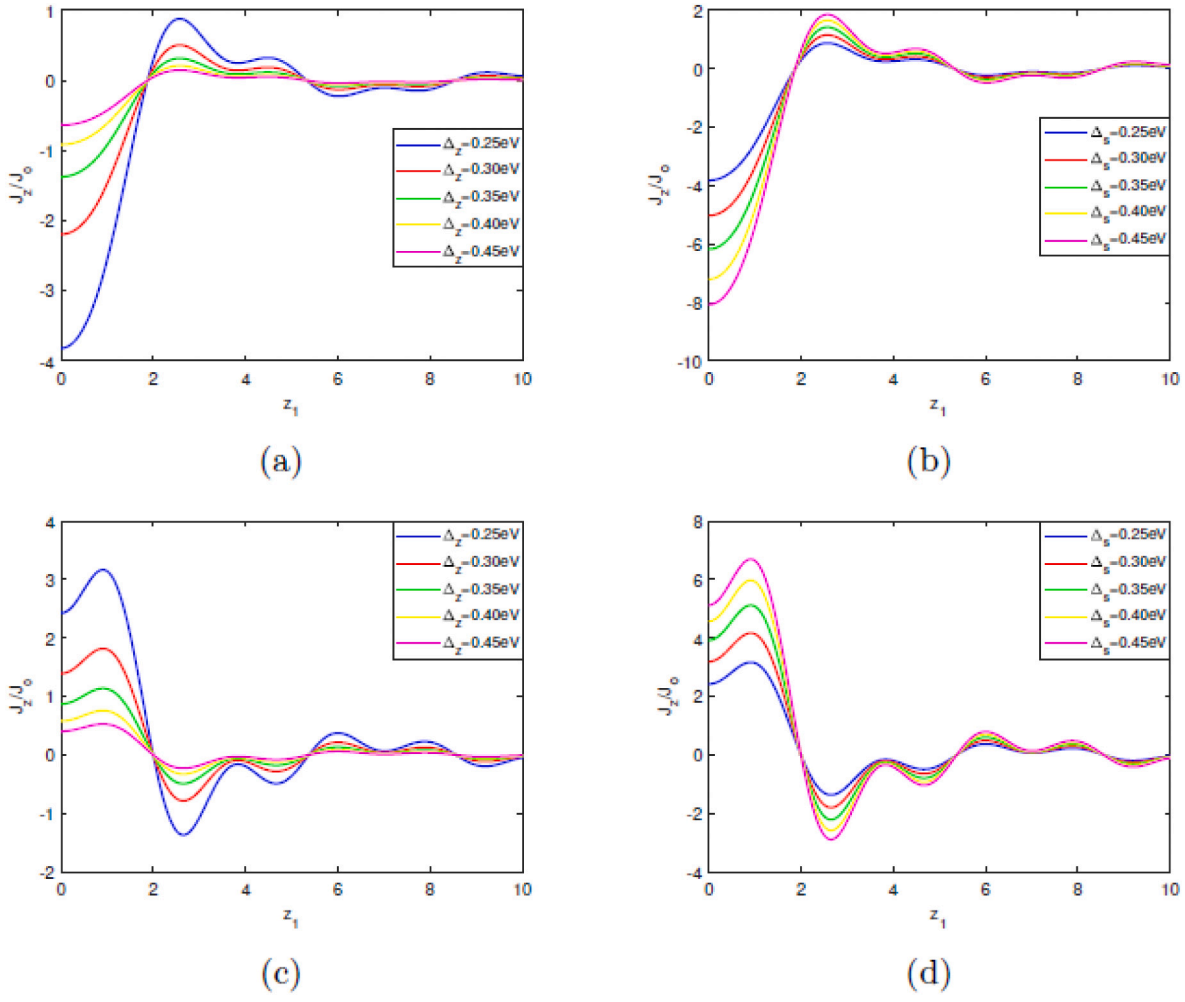

Fig. 3. Dependence of acoustocurrent (J_{zz}^{ae}/J_o^{ae}) on z_1 for different values: (a) Δ_z, $\Omega\tau = 2$ and $\Delta_s = 0.25eV$; (b) Δ_s, $\Omega\tau = 2$, and $\Delta_z = 0.25eV$; (c) Δ_z, $\Omega\tau = 0.5$, and $\Delta_s = 0.25eV$; (d) Δ_s, $\Omega\tau = 0.5$, and $\Delta_z = 0.25$eV.

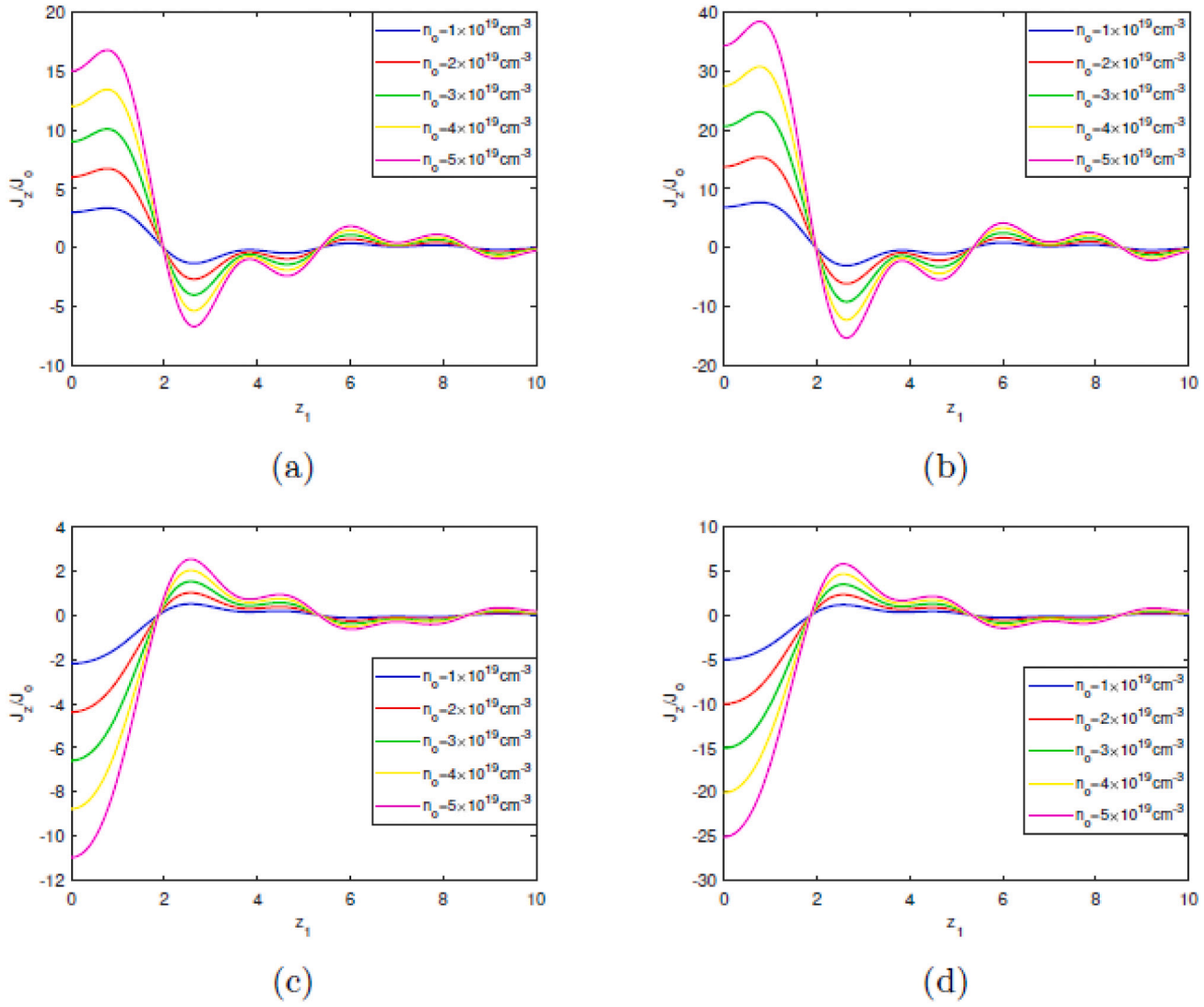

Fig. 4. Dependence of acoustocurrent (J_{zz}^{ae}/J_o^{ae}) }$) on z_1 for different values: (a) n_o, $\Omega\tau = 0.3$, $\Delta_s = 0.25eV$ and $\Delta_z = 0.30eV$; (b) $n_o, \Omega\tau = 0.3$, $\Omega\tau = 0.3$, $\Delta_s = 0.30eV$ and $\Delta_z = 0.25eV$; (c) n_o, $\Omega\tau = 2$, $\Delta_s = 0.25eV$, $\Delta_z = 0.30eV$; (d) n_o, $\Omega\tau = 2$, $\Delta_s = 0.30eV$, $\Delta_z = 0.25eV$.

and the circumferential as

$$J_s = \frac{J_{os}}{2}\left(1 + \sum_{k_1k_2=-\infty}^{\infty}\sum_{\nu_1\nu_2=-\infty}^{\infty}\frac{J_{k_1}(z_1')J_{k_2}(z_2')J_{k_1-\nu_1}(z_1')J_{k_2-\nu_2}(z_2')\langle cos[\nu_2\varphi_o + (\nu_1\omega_1 + \nu_2\omega_2)t]\rangle}{\left[1 + (2\Omega_o + k_1\omega_1 + k_2\omega_2)^2\tau^2\right]}\right.$$
$$-\frac{2\Theta cosAsin(qd_s/2)}{\Delta_s sinAsin(qd_s)}\sum_{k_1k_2=-\infty}^{\infty}\sum_{\nu_1\nu_2=-\infty}^{\infty}J_{k_1}(z_1)J_{k_2}(z_2)J_{k_1-\nu_1}(z_1)J_{k_2-\nu_2}(z_2) \quad (36)$$
$$\left.\times\frac{[\Omega_o + k_1\omega_1 + k_2\omega_2]\tau\langle sin[\nu_2\varphi_o + (\nu_1\omega_1 + \nu_2\omega_2)t]\rangle}{\left[1 + (\Omega_o + k_1\omega_1 + k_2\omega_2)^2\tau^2\right]}\right)cos\vartheta sin\vartheta$$

In order to explain the physical nature of the impact and reveal the unique features of rectification of the ADC dependency on z_1 and z_2 of the fields being mixed, we restricted our further investigation to the significant case of a weak probing field ($\mathscr{E}_2 \ll \mathscr{E}_1$). For the current in the weak signal limit, only particular Bessel function combinations: ($k_2 = 0$, $j = \pm 1$), ($k_2 = \pm 1, j = \mp 1$) and ($k_2 = 0, j = 0$) were used based on the ratio of the frequencies ω_1 and ω_2. Again, we investigated the most important correlations between these pump field mixing frequencies and their harmonic.

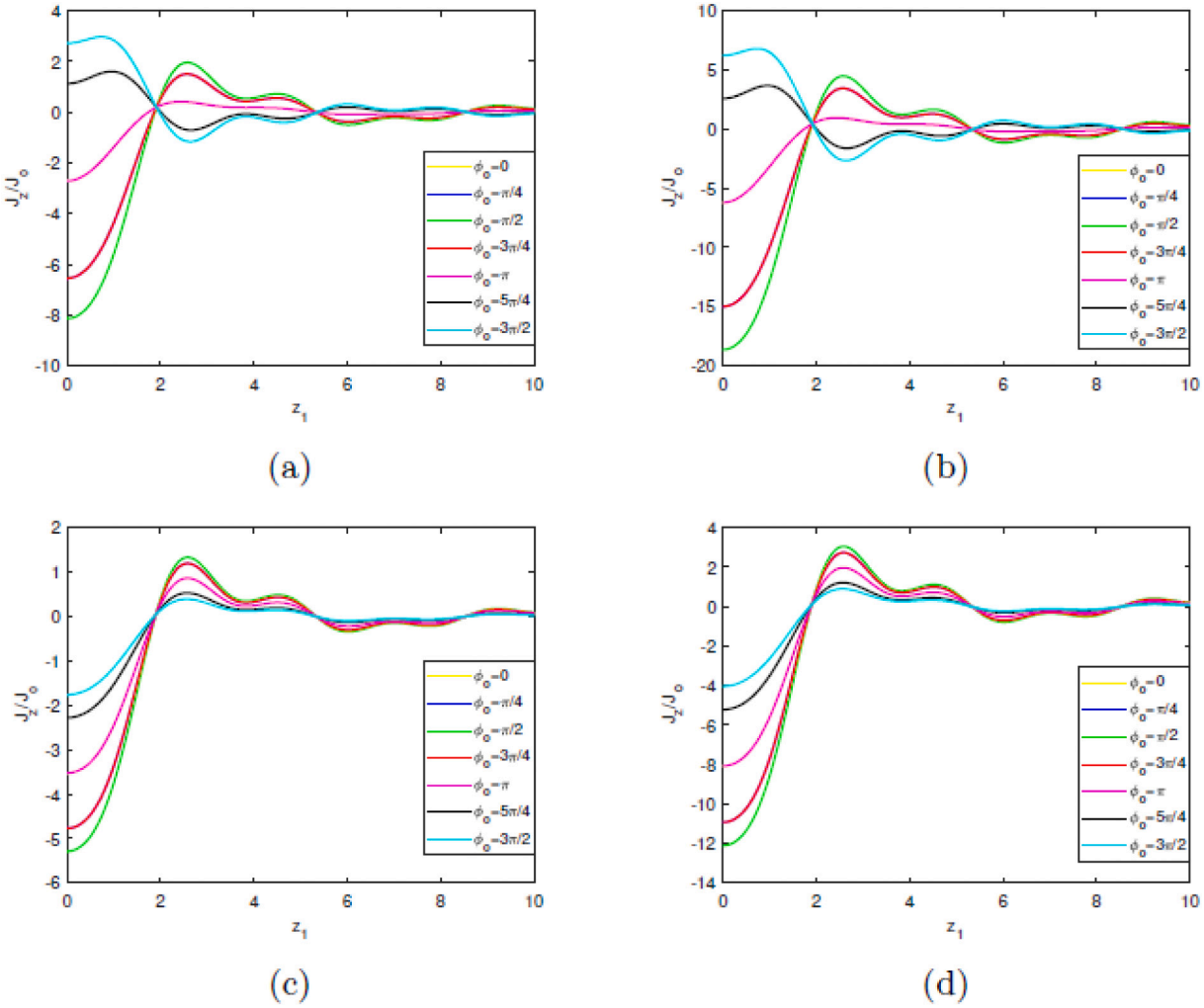

Fig. 5. Dependence of acoustocurrent (J^{ae}_{zz}/J^{ae}_{o}) on z_1 for different values: (a) φ_o, $\Omega\tau = 0.5$, $\Delta_s = 0.25eV$ and $\Delta_z = 0.30eV$; (b) φ_o $\Omega\tau = 0.5$, $\Delta_s = 0.30eV$ $\Delta_z = 0.25eV$ (c) φ_o, $\Omega\tau = 2$, $\Delta_s = 0.25eV$ and $\Delta_z = 0.30eV$; (d) φ_o, $\Omega\tau = 2$, $\Delta_s = 0.30eV$ $\Delta_z = 0.25eV$.

$$
\begin{aligned}
J_z = \frac{J_{oz}}{2}\Bigg(1 + \sum_{k_1k_2=-\infty}^{\infty}\sum_{j=-\infty}^{\infty}\frac{J_{k_1}(z_1')J_{k_2}(z_2')J_{k_1-jm}(z_1')J_{k_2-jn}(z_2')\langle cos[\nu_2\varphi_o + (\nu_1\omega_1+\nu_2\omega_2)t]\rangle}{\left[1+(2\Omega_o + k_1\omega_1 + k_2\omega_2)^2\tau^2\right]} \\
-\frac{2\Theta cosAsin(qd_z/2)}{\Delta_z sinAsin(qd_z)}\sum_{k_1k_2=-\infty}^{\infty}\sum_{j=-\infty}^{\infty}J_{k_1}(z_1)J_{k_2}(z_2)J_{k_1-jm}(z_1)J_{k_2-jn}(z_2) \\
\times\frac{[\Omega_o + k_1\omega_1 + k_2\omega_2]\tau\langle cos[\nu_2\varphi_o + (\nu_1\omega_1+\nu_2\omega_2)t]\rangle}{\left[1+(\Omega_o + k_1\omega_1 + k_2\omega_2)^2\tau^2\right]}\Bigg) \\
+\frac{J_{os}}{2}\Bigg(1 + \sum_{k_1k_2=-\infty}^{\infty}\sum_{j=-\infty}^{\infty}\frac{J_{k_1}(z_1')J_{k_2}(z_2')J_{k_1-jm}(z_1')J_{k_2-jn}(z_2')\langle cos[\nu_2\varphi_o + (\nu_1\omega_1+\nu_2\omega_2)t]\rangle}{\left[1+(2\Omega_o + k_1\omega_1 + k_2\omega_2)^2\tau^2\right]} \\
-\frac{2\Theta cosAsin(qd_s/2)}{\Delta_s sinAsin(qd_s)}\sum_{k_1k_2=-\infty}^{\infty}\sum_{j=-\infty}^{\infty}J_{k_1}(z_1)J_{k_2}(z_2)J_{k_1-jm}(z_1)J_{k_2-jn}(z_2) \\
\times\frac{[\Omega_o + k_1\omega_1 + k_2\omega_2]\tau\langle sin[\nu_2\varphi_o + (\nu_1\omega_1+\nu_2\omega_2)t]\rangle}{\left[1+(\Omega_o + k_1\omega_1 + k_2\omega_2)^2\tau^2\right]}\Bigg)sin^2\vartheta
\end{aligned}
\tag{37}
$$

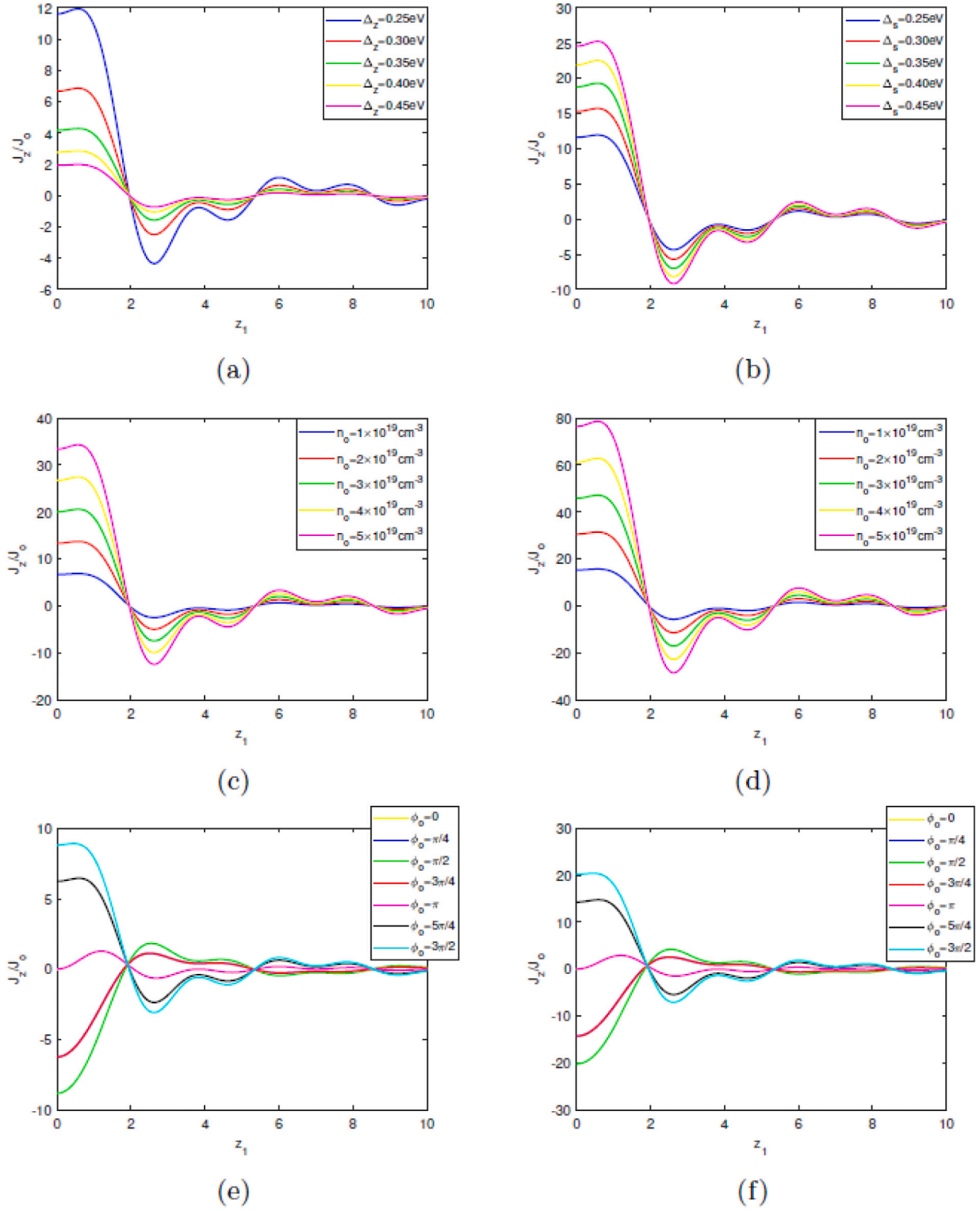

Fig. 6. Dependence of acoustocurrent (J_{zz}^{ae}/J_o^{ae}) on z_1 for different values: (a) Δ_z, $\Delta_s = 0.25eV$ and $n_o = 10^{19}cm^{-3}$; (b) Δ_s, $\Delta_z = 0.25eV$ and $n_o = 10^{19}cm^{-3}$; (c) n_o, $\Delta_s = 0.25eV$, and $\Delta_z = 0.30eV$; (d) n_o, $\Delta_s = 0.30eV$, and $\Delta_z = 0.25eV$; (e) φ_o, $\Delta_s = 0.25eV$, and $\Delta_z = 0.30eV$; (f) φ_o, $\Delta_s = 0.30eV$, and $\Delta_z = 0.25eV$.

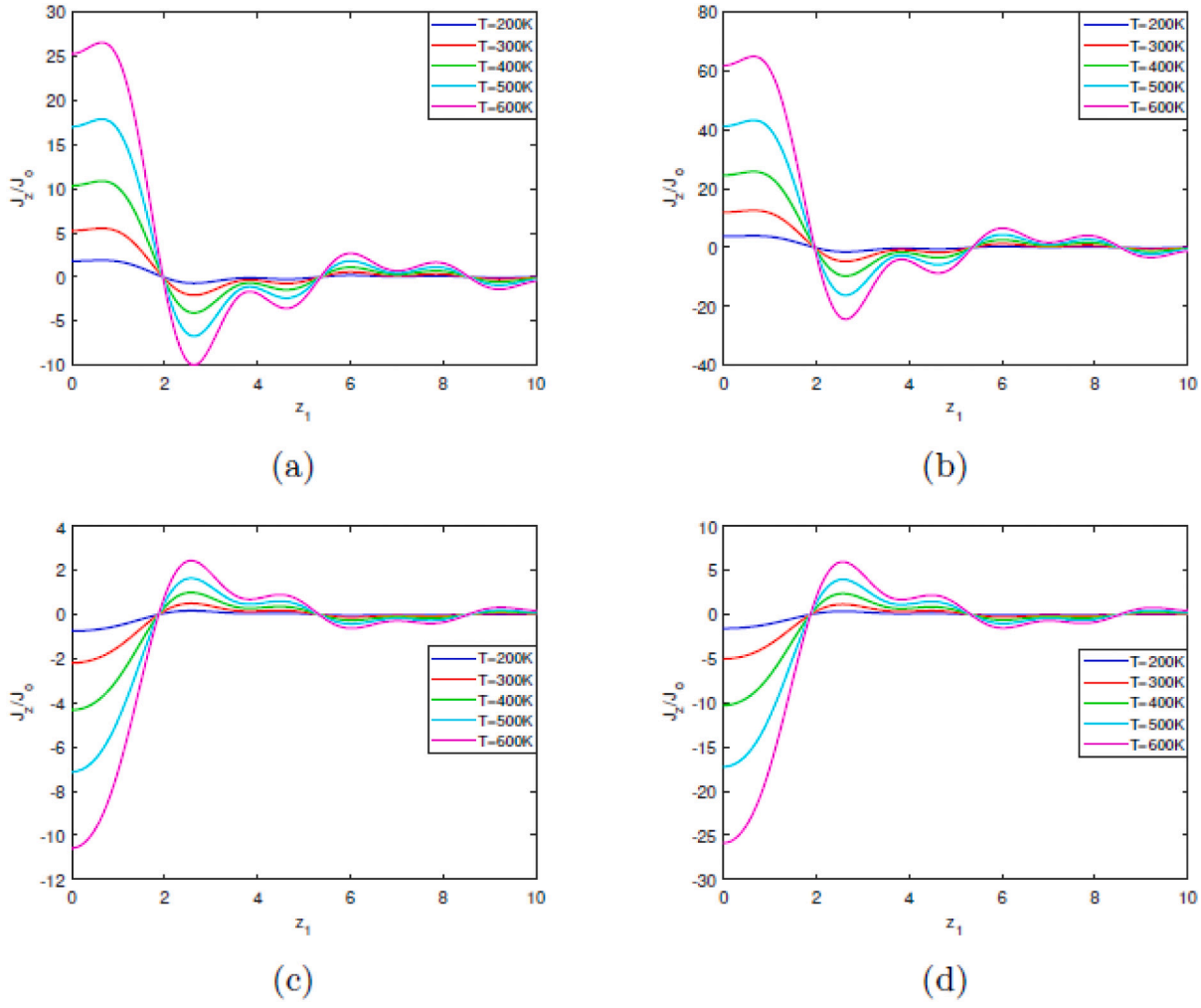

Fig. 7. Dependence of acoustocurrent (J_{zz}^{ae}/J_o^{ae}) on z_1 and z_2 for different values: (a) T, $\Omega\tau = 0.1$, $\Delta_s = 0.25eV$, and $\Delta_z = 0.30eV$; (b) T, $\Omega\tau = 0.1$, $\Delta_s = 0.30eV$ and $\Delta_z = 0.25eV$ (c) T, $\Omega\tau = 2$, $\Delta_s = 0.25eV$, and $\Delta_z = 0.30eV$; (d) T, $\Omega\tau = 2$, $\Delta_s = 0.30eV$ and $\Delta_z = 0.25eV$.

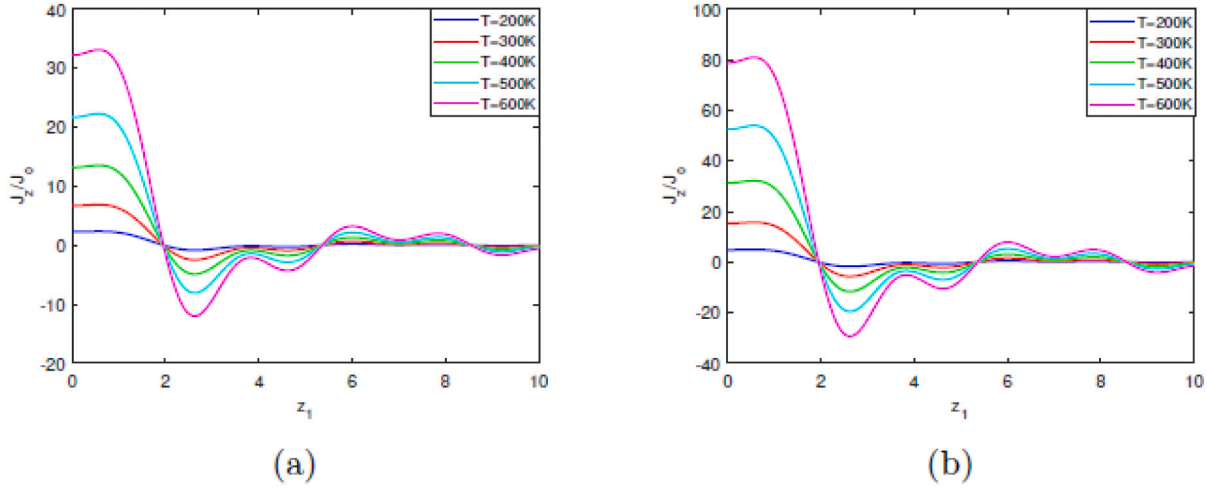

Fig. 8. Dependence of acoustocurrent (J_{zz}^{ae}/J_o^{ae}) on z_1 and z_2 for different values: (a) T, $\Delta_s = 0.25eV$, and $\Delta_z = 0.30eV$; (b) T, $\Delta_s = 0.30eV$, and $\Delta_z = 0.25eV$.

and

$$J_s = \frac{J_{os}}{2}\left(1 + \sum_{k_1k_2=-\infty}^{\infty}\sum_{j=-\infty}^{\infty}\frac{J_{k_1}(z_1')J_{k_2}(z_2')J_{k_1-jm}(z_1')J_{k_2-jn}(z_2')\langle cos[\nu_2\varphi_o + (\nu_1\omega_1+\nu_2\omega_2)t]\rangle}{\left[1+(2\Omega_o+k_1\omega_1+k_2\omega_2)^2\tau^2\right]}\right.$$
$$-\frac{2\Theta cosAsin(qd_s/2)}{\Delta_s sinAsin(qd_s)}\sum_{k_1k_2=-\infty}^{\infty}\sum_{\nu_1\nu_2=-\infty}^{\infty}J_{k_1}(z_1)J_{k_2}(z_2)J_{k_1-jm}(z_1)J_{k_2-jn}(z_2) \quad (38)$$
$$\left.\times\frac{[\Omega_o+k_1\omega_1+k_2\omega_2]\tau\langle sin[\nu_2\varphi_o+(\nu_1\omega_1+\nu_2\omega_2)t]\rangle}{\left[1+(\Omega_o+k_1\omega_1+k_2\omega_2)^2\tau^2\right]}\right)cos\vartheta sin\vartheta$$

where $\nu_1 = jm$, $\nu_2 = jn$, $z' = 2z = 2e\mathscr{E}_i d_{s,z}/\omega_i$ $(i = 1, 2)$ and $\Omega_o = \Omega = e\mathscr{E}_o d_{s,z}$ is the Bloch frequency.

3. Results and discussion

The rectification of sinusoidal signals in FSWCNT, due to the mixing of two coherent electromagnetic waves of phase difference φ_o with commensurate frequencies of $\omega_1 = \Omega$ and $\omega_2 = 2\Omega$ was investigated theoretically, by invoking the semiclassical conditions in the hypersound regime. The general equations for the rectified acoustoelectric direct current density in FSWCNT were presented in Eqs. (37) and (38), respectively but of most interest to us was the axial component in Eq. (37). The ADC generated in the presence of acoustic phonons in both cases were observed to be strongly dependent on the acoustic wavenumber (q), frequency (ω_q), temperature (T) and external electric field $\mathscr{E}$. A transparency window was observed when $\omega_q \gg 2\Delta_s sin(qd_s/2)$ and $\omega_q \gg 2\Delta_s sin(qd_z/2)$, which was as a consequence of the conservation laws of energy and momentum. The implication was that the acoustic phonons could only interact with carriers whose momenta were $\hbar q/2$. If the frequency of the sound flux going through the sample was exceedingly high, there would be no sound absorption and there would be no acoustoelectric current density (J_{zz}^{ae}/J_o^{ae}).

At this juncture, we explain the Physics of the strong electrodynamic potential generated as a result of the deformation potential coupling in the FSWCNT. The intricate band structure of FSWCNTs causes the deformation potential coupling. The carrier energy levels separate into various energy bands in the presence of the FSWCNT's crystal potential, which results from the atoms in the lattice. The atoms are displaced from their equilibrium positions as the acoustic wave travels through the FSWCNT. The carriers' crystal potential and the carrier energy bands that result from the potential are both distorted or deformed as a result of this displacement. A deformation potential tensor ensues and which can be used for short and long-wavelength acoustic phonons to account for the deformation of the energy bands in the FSWCNT as:

$$\delta\varepsilon = \frac{\partial}{\partial x_i}\Lambda_{ij}\xi_j = ik\Lambda_{ij}\xi_j. \quad (39)$$

where $\delta\varepsilon$ is the change in energy, Λ_{ij} is the deformation potential tensor and ξ is the acoustic wave displacement (i.e., $\xi = \xi_o e^{i(\vec{k}\cdot\vec{r}-\omega t)}$). Since the change of energy of the carrier in the energy band is spatially dependent, a net force based on the Hooke's is exerted on the carriers because of the presence of the acoustic wave as:

$$F_\ell = -\frac{\partial}{\partial x_\ell}\delta\varepsilon = k^2\Lambda_{\ell j}\xi_j \quad (40)$$

As a result, in this case, the deformation potential couples the carriers to the acoustic wave strongly, and the higher the carrier density, the stronger the coupling between the acoustic phonons and carrier yielding the acoustoelectric current. The coupling is proportional to both the magnitude of the deformation potential constant and the square of the acoustic phonons wave number (q). The deformation potential constant in the majority of interesting materials is on the scale of several electron volts. This coupling mechanism predominates in the majority of conducting solids at high enough frequencies due to its frequency dependency. At frequencies in the megacycle range, this mechanism predominates the electron-phonon interaction in the majority of high-resistivity semiconductors, and even when the acoustic waves are transverse, the forces resulting from the deformation potential are always longitudinal.

Fig. 2 illustrated the dependency of the ADC (J_{zz}^{ae}/J_o^{ae}) on the dimensionless ac fields z_1 and z_2 for different values of $\Omega\tau$ when $\Delta_s = 0.25eV$ $\Delta_z = 0.30eV$ (see Fig. 2(a)) and $\Delta_s = 0.30eV$ $\Delta_z = 0.25eV$ (see Fig. 1(b)). We observed that J_{zz}^{ae}/J_o^{ae} was initially high at $z_1 = 0$ and $z_2 = 0.4$. J_{zz}^{ae}/J_o^{ae} increased slightly for increasing z_1 until it reached its maximum value. Further increase in z_1 resulted in the decrease in the magnitude of J_{zz}^{ae}/J_o^{ae} in a monotonic manner until it reached its minimum value. Increasing $\Omega\tau$ resulted in a decrease in magnitude of J_{zz}^{ae}/J_o^{ae} up to $\Omega\tau = 0.8$. This is because the presence of the dc electric field also affects the motion of the electrons. The electric field acts to transfer energy to the carrier system, so that the distribution is shifted to higher energies in the presence of the electric field than in its absence. In the absence of the electric field, the carriers occupy states of low energies, whereas states of higher energy are vacant. Therefore, the carriers are more likely to absorb a phonon than to emit one, since in the former process they would go from the highly occupied states of low energy to the nearly vacant states of higher energy, whereas for the latter process they would have to do the reverse. The electric field shifts the carrier distribution in such a way that states of higher energy become occupied, whereas states of lower energy become vacant. Thus, the probability for absorption of phonons decreases, and the probability of emission of phonons increases. As the probability for absorption of phonons decreases, the carrier-phonon coupling is weak and the deformation potential constant is low and thus, the ADC generated is low as $\Omega\tau$ increases.

Further increase in $\Omega\tau$ ($\Omega\tau > 1$) resulted in a reversal of the direction (i.e., negative) and increased the magnitude of J_{zz}^{ae}/J_o^{ae}. The ADC was strongly nonlinear and non-ohmic but dependent on $\Omega\tau$. Moreover, for $z_1 > 2$ we observed a dramatic decrease in the ADC generated which oscillated weakly in both directions which indicated that, at high frequencies the rectification was nearly smooth as against the case of low frequency. The decrease in magnitude of J_{zz}^{ae}/J_o^{ae} observed was due to the increase in scattering as the carriers performed Bloch oscillations thus, the region with negative differential conductivity (NDC) i.e., $\partial J_{zz}^{ae}/\partial z_1 < 0$. Fig. 2(a) and (b) demonstrated similar behaviour but the magnitude of J_{zz}^{ae}/J_o^{ae} obtained in Fig. 2(b) was twice that obtained in Fig. 1(a). The difference being that carrier coupling with acoustic phonons when $\Delta_s = 0.30eV$ $\Delta_z = 0.25eV$ (see Fig. 2(b)) was much stronger and so generated a higher deformation potential constant and thus, a higher ADC was obtained than when $\Delta_s = 0.25eV$ $\Delta_z = 0.30eV$ (see Fig. 2

(a)). Thus, more carriers interacted strongly with the acoustic phonons to generate a high intraminiband ADC for $\Delta_s = 0.30eV\ \Delta_z = 0.25eV$ (see Fig. 2(b)) than for $\Delta_s = 0.25eV\ \Delta_z = 0.30eV$ (see Fig. 2(b)).

We investigated in Fig. 3 the dependency of J_{zz}^{ae}/J_o^{ae} on z_1 and z_2 for varied values of Δ_s and Δ_s. Fig. 3(a) and (b) demonstrated the behaviour when Δ_z was varied for $\Omega\tau = 2$, and Δ_s was fixed ($\Delta_s = 0.25eV$ see Fig. 3 (a)) and when Δ_s was varied for $\Omega\tau = 2$, and Δ_z was fixed ($\Delta_z = 0.25eV$ see Fig. 3(b)). It was observed in Fig. 3(a) and (b) that the direction of the rectified ADC was reversed. This reversal was due to the fact that the coupling of the carriers with the acoustic phonons was very strong and thus, generated a high deformation potential constant which is strongly dependent on the magnitude of the deformation potential constant and square of the acoustic phonons wavenumber and a high acoustoelectric field. The acoustoelectric field generated opposed the direction of the external bichromatic electric field which resulted in the reversal of the ADC.

In effect the scattering was stronger when Δ_z was varied for $\Omega\tau = 2$, and Δ_s was fixed ($\Delta_s = 0.25eV$) which generated a low J_{zz}^{ae}/J_o^{ae} (see Fig. 3 (a)) than when Δ_s was varied for $\Omega\tau = 2$, and Δ_z was fixed ($\Delta_z = 0.25eV$) which generated a high rectified ADC (see Fig. 3(b)). Furthermore, Fig. 3 (c) and (d) demonstrated the behaviour when Δ_z was varied for $\Omega\tau = 0.5$, and Δ_s was fixed ($\Delta_s = 0.25eV$ see Fig. 3(c)) and when Δ_s was varied for $\Omega\tau = 0.5$, and Δ_z was fixed ($\Delta_z = 0.25eV$ see Fig. 3(d)). We observed from their behaviour that for weak static field ($E_o < 1$), the direction of the ADC generated was reversed. This means the acoustoelectric field generated from the carrier-phonon coupling was in the same direction as the external bichromatic field. However, the ADC was high when Δ_z was varied for $\Omega\tau = 0.5$, and Δ_s was fixed (i.e. $\Delta_s = 0.25$ see Fig. 3(c)) than when Δ_s was varied for $\Omega\tau = 0.5$, and Δ_z fixed (i.e. $\Delta_z = 0.25$ see Fig. 3 (c)).

Fig. 4 displayed the ADC (J_{zz}^{ae}/J_o^{ae}) dependency on z_1 and z_2 for different values of carrier/impurity concentration (n_o) when $\Omega\tau = 0.3$, $\Delta_s = 0.25eV$ and $\Delta_z = 0.30eV$ (see Fig. 4(a)) and $\Omega\tau = 0.3$, $\Delta_s = 0.30eV$ and $\Delta_z = 0.25eV$ (see Fig. 4(b)). In the presence weak static field coupled with scattering, as the carrier density (n_o) was increased, a high ADC was generated as well. The ADC obtained for $\Omega\tau = 0.3$, $\Delta_s = 0.25eV$ and $\Delta_z = 0.30eV$ (see Fig. 4(a)) was lower than that obtained for $\Omega\tau = 0.3$, $\Delta_s = 0.30eV$ and $\Delta_z = 0.25eV$ (see Fig. 4(b)). This was attributed to the fact that there were more carriers which interacted strongly with the acoustic phonons along the base helix where scattering of carriers by energetic phonons were less comparable to the tubular direction where more energetic phonons scattered the carriers. Similar behaviour was observed in Fig.4(c) and (d) but the direction of the rectified ADC was reversed due to the direction of the acoustoelectric field (see Fig. 4(c) and (d)).

Using the same set of values as in Fig. 4, we investigated and observed a similar but interesting behaviour in Fig. 5 for varied values of φ_o when $\Omega\tau = 0.5$, $n_o = 10^{19}cm^{-3}$, $\Delta_s = 0.25eV$ and $\Delta_z = 0.30eV$ (see Fig. 5(a)) and $\Omega\tau = 0.5$, $n_o = 10^{19}cm^{-3}$, $\Delta_s = 0.30eV\ \Delta_z = 0.25eV$ (see Fig. 5(b)). It was convenient to illustrate the dependence of the direction and magnitude of the rectified ADC on the relative phase φ_o in the case of mixing of harmonics. It could be seen from Eq. (37) that the dependence on the phase was determined only by the factor $cos\varphi_o$. Consequently, for φ_o the rectified ADC attained its maximal value for $\pi/2$ phase difference and vanishes when the phase difference was zero. Accordingly, by changing the phase, we could change not only the magnitude, but also the direction of the rectified current. In particular, when the phase difference between the fields assumed values of $\pi/2$ and $3\pi/2$, the direction of current was reversed. Changing the phase value resulted in only specific combination of the harmonics which contributed to the rectification. For $\varphi_o = \pi/2$ we have the sixth harmonic, $\varphi_o = 3\pi/4$ yield the fourth harmonic and $\varphi_o = 3\pi/2$ yielded the second harmonic. However, a high conductivity was obtained when $\Omega\tau = 0.5$, $n_o = 10^{19}cm^{-3}$, $\Delta_s = 0.30eV$ and $\Delta_z = 0.25eV$ (see Fig. 5(b)) than when $\Omega\tau = 0.5$, $n_o = 10^{19}cm^{-3}$, $\Delta_s = 0.25eV$ and $\Delta_z = 0.30eV$ (see Fig. 5(a)). Also when $\Omega\tau = 0.5$, $n_o = 10^{19}cm^{-3}$, $\Delta_s = 0.25eV$ and $\Delta_z = 0.30eV$ we obtained a low ADC condutivity due to the strong scattering along this direction (see Fig. 5(c)) than when $\Omega\tau = 0.5$, $n_o = 10^{19}cm^{-3}$, $\Delta_s = 0.30eV$ and $\Delta_z = 0.25eV$ which yielded a high ADC (see Fig. 5(d)). An analogous dependence was also typical of other ratios of frequencies of the fields being mixed. It should be noted for experimental observation that, it is important to maintain a constant phase difference of the fields being mixed. Experimental methods for maintaining a constant phase difference of microwave fields were considered in ref. [25]. It could be seen that the conductivity of the FSWCNT strongly depended on the frequency of the pump field; and as we passed to the high frequency limit $\omega\tau \gg 1$, conductivity tends to zero for any harmonic.

We consider the case we are interested in when the static pump field is absent ($\mathscr{E}_o = 0$). For a purely ac mixing, we obtained the rectified ADC as;

$$
\begin{aligned}
J_z = \frac{J_{oz}}{2}\Bigg(1 + \sum_{k_1k_2=-\infty}^{\infty}\sum_{j=-\infty}^{\infty}\frac{J_{k_1}(z_1')J_{k_2}(z_2')J_{k_1-jm}(z_1')J_{k_2-jn}(z_2')\langle cos[\nu_2\varphi_o + (\nu_1\omega_1 + \nu_2\omega_2)t]\rangle}{\left[1 + (k_1\omega_1 + k_2\omega_2)^2\tau^2\right]} \\
-\frac{2\Theta cosAsin(qd_z/2)}{\Delta_z sinAsin(qd_z)}\sum_{k_1k_2=-\infty}^{\infty}\sum_{j=-\infty}^{\infty}J_{k_1}(z_1)J_{k_2}(z_2)J_{k_1-jm}(z_1)J_{k_2-jn}(z_2) \\
\times\frac{[k_1\omega_1 + k_2\omega_2]\tau\langle cos[\nu_2\varphi_o + (\nu_1\omega_1 + \nu_2\omega_2)t]\rangle}{\left[1 + (k_1\omega_1 + k_2\omega_2)^2\tau^2\right]}\Bigg) \\
+\frac{J_{os}}{2}\Bigg(1 + \sum_{k_1k_2=-\infty}^{\infty}\sum_{j=-\infty}^{\infty}\frac{J_{k_1}(z_1')J_{k_2}(z_2')J_{k_1-jm}(z_1')J_{k_2-jn}(z_2')\langle cos[\nu_2\varphi_o + (\nu_1\omega_1 + \nu_2\omega_2)t]\rangle}{\left[1 + (k_1\omega_1 + k_2\omega_2)^2\tau^2\right]} \\
-\frac{2\Theta cosAsin(qd_s/2)}{\Delta_s sinAsin(qd_s)}\sum_{k_1k_2=-\infty}^{\infty}\sum_{j=-\infty}^{\infty}J_{k_1}(z_1)J_{k_2}(z_2)J_{k_1-jm}(z_1)J_{k_2-jn}(z_2) \\
\times\frac{[k_1\omega_1 + k_2\omega_2]\tau\langle sin[\nu_2\varphi_o + (\nu_1\omega_1 + \nu_2\omega_2)t]\rangle}{\left[1 + (k_1\omega_1 + k_2\omega_2)^2\tau^2\right]}\Bigg)sin^2\vartheta
\end{aligned}
\tag{41}
$$

This formula implied that in the case of mixing of the pump field with its odd harmonic, ADC is not induced in the system, while in the case of even harmonics, such a current always exists. It is noteworthy that, it

was even harmonics that can be used most effectively to enhance THz radiation because the parametric enhancement effect was not suppressed in this case by the generation of pump field harmonics.

Fig. 6 showed the ADC density (J_{zz}^{ae}/J_{o}^{ae}) dependency on z_1 and z_2 for different values of Δ_z, Δ_s, n_o and φ_o for a purely ac mixing of the harmonics when $E_o = 0$. The rectified ADC density obtained in the absence of the static field of the pump was higher when compared with that in the presence of the field. The observed non-ohmicity in the I-V characteristic of the FSWCNT's rectified ADC (J_{zz}^{ae}/J_{o}^{ae}) could be attributed to the Bloch oscillation of the carriers due to the high non-parabolicity of the FSWCNT's band structure and Stark component (summation over k). It is worthwhile to note that $\Omega\tau_{max}$ could be used to determine the relaxation time of the dominant type of scattering (i.e. electron-phonon) in the FSWCNT.

Furthermore, we investigated the dependency of J_{zz}^{ae}/J_{o}^{ae} on z_1 and z_2 for different values of temperature when $\Omega\tau \ll 1$ and $\Omega\tau \gg 1$. Fig. 7(a) and (b) we observed that the rectified ADC increase as the temperature increases for $\Omega\tau \ll 1$ as in Ref. [31]. This is because increasing temperature decrease the band gap of the FSWCNT and thus, more electrons with enough energy and momentum can jump the band gap and interacts strongly with the acoustic phonons to generate a high deformation potential and a high ADC as a result. The rectified ADC generated when $\Delta_s = 0.25eV$ and $\Delta_z = 0.30eV$ (see Fig. 7(a)) was high and double that obtained for $\Delta_s = 0.30eV$ and $\Delta_z = 0.25eV$ (see Fig. 7(b)). When $\Omega\tau \gg 1$, we observed that the rectified ADC is reversed but the ADC generated was not as high as that obtained in Fig. 7(a) and (b). When $\Omega\tau = 2$, $\Delta_s = 0.25eV$ and $\Delta_z = 0.30eV$ (see Fig. 7(c)) was high and double that obtained for $\Delta_s = 0.30eV$ and $\Delta_z = 0.25eV$ (see Fig. 7(d)).

Furthermore, we showed the ADC density (J_{zz}^{ae}/J_{o}^{ae}) dependency on z_1 and z_2 for different values of Δ_z, and Δ_s for a purely ac mixing of the harmonics when $E_o = 0$ (see Fig. 8(a) and (b)). It is observed that increasing the temperature minimises or reduces the band gap of the FSWCNT along the axial direction. This gives more carriers enough energy and momentum to jump the band gap into the conduction band. Again, increasing the F-dopants add more states to the band structure which increases the carrier concentration in the conduction band. These carriers in both cases are coupled strongly with the acoustic phonons via the deformation potential constant to generate the ADC (see Figs. 4 and 7). As varying n_o and T influences the magnitude of the ADC in both direction, this will go a long way to increase the output current (ADC), output power and the efficiency of the FSWCNT as an acoustoelectric device (see Figs. 4, 7 and 8).

As to why we chose fluorine-doped SWCNTs to elements like Cl, Br, and I was due to FSWCNT's semiconducting properties. Tabrowski et al. conducted investigation into the doping of SWCNTs with halogenated solvents (i.e., dichloromethane, chloroform and bromoform) [32]. They found out that, using halogenated solvents as the medium significantly enhances the carrier conductivity at room temperature. For SWCNT films made in an acetone/toluene mixture had a carrier conductivity of $853 \pm 62\ Scm^{-1}$ [33], but when dichloromethane and chloroform were used, the carrier conductivity increased to $1652 \pm 186\ Scm^{-1}$ and $1966 \pm 425\ Scm^{-1}$, respectively. The Br-SWCNT specimen created in bromoform shows an even more noticeable rise. The Br-SWCNT's carrier conductivity increases were quadrupled in comparison to the material made utilising non-halogen solvents, reaching $3819 \pm 241\ Scm^{-1}$. The measured values were quite high despite the mild chemical nature of these molecules [34].

The carrier conductivity which reduced as temperature rises, indicated that the SWCNT networks were basically metallic in nature [34]. Due to this, the Seebeck coefficient values of variously produced SWCNT films were adequate but not outstanding. The doped-SWCNT room temperature Seebeck coefficient of $46 \pm 3\mu V/K$ matched the performance of other undoped SWCNT-based thermogenerators [35]. In contrast, the Seebeck coefficients for the ensembles made in dichloromethane (SWCNT/DCM), chloroform (SWCNT/CF), and bromoform (SWCNT/BF) were 26 ± 2, 22 ± 3, and $19 \pm 1\mu V/K$, respectively. Therefore, the observed drop in Seebeck coefficients strongly suggests that the material was doped when processed using these halogenated aromatic solvents on a regular basis. The doping changed the material from non-degenerate to degenerate character, which had a significant impact on the carrier conductivity but a detrimental impact on the thermoelectric power [36]. The doping also increased the carrier concentration and added more state to the already existing bandstructure. The increase in carrier conductivities brought on by doping was responsible for the decline in Seebeck coefficients.

Furthermore, bromoform, which had the lowest electric dipole moment of 0.990 Debye compared to 1.010 and 1.600 Debye for chloroform and dichloromethane, respectively, was most likely to produce the halogen moieties that could dope SWCNT films. This explained why bromoform had the greatest improvement of carrier conductivity [37]. As opposed to F-doped SWCNTs which are more semiconducting, heavier halogenated solvents (i.e. Cl, Br, and I) significantly inhibited the semiconducting character by adding states (i.e., increase in impurity concentration) and moving the Fermi level to the middle of the band and thus, flipping the SWCNT from non-degenerate (semiconducting) to degenerate (metallic) character. The semiconducting character was significantly reduced, especially in the Br-doped SWCNT film. This effect resulted from the addition of an impurity band close to the Fermi level, which altered the chemical potential and reduced the band gap from semiconducting to metallic [38]. As a result, the materials (SWCNTs) become more metallic when Cl, Br and I are added in that order. They came to the conclusion that the improvement in carrier conductivity with halogens was probably caused by a change in the chemical potentials of the SWCNT films [32] which increased the carrier conductivity but reduced the thermoelectric power [32].

The one-dimensional semiconducting FSWCNT benefits from the ADC effect because, a "high-frequency-induced phase-dependent dc current by Bloch oscillator non-ohmicity" using a bichromatic field has been observed by Seeger and co-workers in 3- dimensional superlattice (SL) [39], Seidu et al. in quasi-one dimensional SWCNT [19] and Mensah et al. in nonparabolic semiconductor.

4. Conclusion

We studied the ADC generation due to mixing of waves associated with commensurate harmonics theoretically using a tractable analytical approach in the hypersound regime. The rectified ADC obtained was strongly nonlinear and non-ohmic. Numerous causes may be responsible for the FSWCNT's non-ohmicity in the I-V characteristic including the non-parabolic band energy-momentum relation, carrier heating, stark component, and Bloch oscillations of intraminiband carriers. It was possible to change the magnitude and direction of the generated ADC. Generation of the ADC corresponded to even instability regions in the FSWCNT. This work, in our opinion, will inspire fresh research and the development of new tools for the rectification and detection of THz radiation. Thus, based on the high ADC obtained, we propose FSWCNT for ADC generation under bichromatic fields with commensurate frequencies.

Declaration of competing interest

The authors declare no conflict of interest in processing this manuscript.

Data availability

The data that supports the findings of this study are available within the article.

References

[1] K. Hofbeck, J. Grenzer, E. Schomburg, A.A. Ignatov, K.F. Renk, D.G. Pavel'ev, Yu. Koschurinov, et al., High-frequency self-sustained current oscillation in an Esaki-Tsu superlattice monitored via microwave emission, Phys. Lett. A 218 (3–6) (1996) 349–353.

[2] Walter Schneider, Karlheinz Seeger, Harmonic mixing of microwaves by warm electrons in germanium, Appl. Phys. Lett. 8 (6) (1966) 133–135.

[3] I.U.A. Romanov, Nonlinear effects in periodic semiconductor structures(Frequency multiplication due to nonparabolicity of dispersion law in semiconductor structure subbands, noting electromagnetic signal transformation), Opt. Spektroskopiia 33 (1972) 917–920.

[4] Leo Esaki, Ray Tsu, Superlattice and negative differential conductivity in semiconductors, IBM J. Res. Dev. 14 (1) (1970) 61–65.

[5] Andreas Wacker, Semiconductor superlattices: a model system for nonlinear transport, Phys. Rep. 357 (1) (2002) 1–111.

[6] Peter Reimann, Brownian motors: noisy transport far from equilibrium, Phys. Rep. 361 (2–4) (2002) 57–265.

[7] A.V. Shorokhov, N.N. Khvastunov, T. Hyart, K.N. Alekseev, Generation of direct current in a semiconductor superlattice under the action of a bichromatic field as a parametric effect, J. Exp. Theor. Phys. 111 (5) (2010) 822–829.

[8] B. Ferguson, X.C. Zhang, Terahertz magnetic response from artificial materials, Nat. Mater. 1 (2002) 26–33.

[9] Masayoshi Tonouchi, Cutting-edge terahertz technology, Nat. Photonics 1 (2) (2007) 97–105.

[10] A.V. Shorokhov, Kirill N. Alekseev, Quantum derivatives and terahertz gain in a superlattice, J. Exp. Theor. Phys. 105 (1) (2007) 198–200.

[11] Iu.A. Romanov, Upwards parametric frequency transformation in superlattices, Radiofizika 23 (5) (1980) 617–625.

[12] Yu.A. Romanov, Yu. Romanova, Bloch oscillations in superlattices: the problem of a terahertz oscillator, Semiconductors 39 (1) (2005) 147–155.

[13] Timo Hyart, Tunable Superlattice Amplifiers Based on Dynamics of Miniband Electrons in Electric and Magnetic Fields, University of Oulu, Finland, 2009. PhD diss., Dissertation.

[14] S.S. Abukari, S.Y. Mensah, N.G. Mensah, K.A. Dompreh, A. Twum, F.K.A. Allotey, Direct Current Generation Due to Wave Mixing in Zigzag Carbon Nanotubes, arXiv preprint arXiv:1007.1772, 2010.

[15] K.N. Alekseev, M.V. Gorkunov, N.V. Demarina, T. Hyart, N.V. Alexeeva, A. V. Shorokhov, Europhys. Lett. 73 (2006) 934.

[16] Yuriy A. Romanov, Julia Yu Romanova, Lev G. Mourokh, Semiconductor superlattice in a biharmonic field: absolute negative conductivity and static electric-field generation, J. Appl. Phys. 99 (1) (2006), 013707.

[17] A.V. Shorokhov, K.N. Alekseev, Physica E 33 (2006) 284.

[18] A.A. Zharov, E.P. Dodin, A.S. Raspopin, Compression of terahertz radiation in resonant systems with a quantum superlattice, J. Exp. Theor. Phys. Lett. 72 (9) (2000) 453–456.

[19] Sulemana S. Abukari, Kofi W. Adu, Samuel Y. Mensah, Natalia G. Mensah, Musah Rabiu, Anthony Twum, Mathew Amekpewu, Kwadwo A. Dompreh, Rectification due to harmonic mixing of two coherent electromagnetic waves with commensurate frequencies in carbon nanotubes, Eur. Phys. J. B 86 (3) (2013) 1–4.

[20] S. Mensah, G.M. Shmelev, É.M. Épshtein, Izv. Vyssh. Uchebn. Zaved., Fiz. 6 (1988) 112.

[21] D. Sekyi-Arthur, C. Jebuni-Adanu, S.Y. Mensah, Thermal conductivity in fluorine-doped single-walled carbon nanotubes, Materialia 26 (2022) 101613.

[22] D. Sakyi-Arthur, S.Y. Mensah, N.G. Mensah, K.A. Dompreh, R. Edziah, in: Absorption of Acoustic Phonons in Fluorinated Carbon Nanotube with Non-parabolic, Double Periodic Band. Phonons in Low Dimensional Structures, InTech, 2018, pp. 129–142, https://doi.org/10.5772/intechopen.78231.

[23] D. Sakyi-Arthur, S.Y. Mensah, K.W. Adu, K.A. Dompreh, R. Edziah, N.G. Mensah, C. Jebuni-Adanu, Induced hall-like current by acoustic phonons in semiconductor fluorinated carbon nanotube, World J. Condens. Matter Phys. 10 (2020) 71–87, https://doi.org/10.4236/wjcmp.2020.102005.

[24] D. Sakyi-Arthur, S.Y. Mensah, K.W. Adu, K.A. Dompreh, R. Edziah, N.G. Mensah, Acoustoelectric effect in fluorinated carbon nanotube in the absence of external electric field, World J. Condens. Matter Phys. 10 (2020) 1–11, https://doi.org/10.4236/wjcmp.2020.101001.

[25] D. Sakyi-Arthur, S.Y. Mensah, K.W. Adu, K.A. Dompreh, R. Edziah, N.G. Mensah, C. Jebuni-Adanu, Semiconductor fluorinated carbon nanotube as a low voltage current amplifier acoustic device, World J. Condens. Matter Phys. 10 (2020) 12–26, https://doi.org/10.4236/wjcmp.2020.101002.

[26] D. Sakyi-Arthur, S.Y. Mensah, N.G. Mensah, K.W. Adu, K.A. Dompreh, R. Edziah, Tunable power factor in fluorine-doped single-walled carbon nanotubes, J. Appl. Phys. 128 (24) (2020), 244301.

[27] D. Sekyi-Arthur, M. Egblewogbe, S.Y. Mensah, N.G. Mensah, K.W. Adu, K. A. Dompreh, R. Edziah, S. Atarah, Giant thermoelectric figure of merit in fluorine-doped single walled-carbon nanotubes, Physica E 142 (2022) 115292. https://doi.org/10.1016/j.physe.2022.115292.

[28] D. Sekyi-Arthur, S.Y. Mensah, K.A. Dompreh, G. Nkrumah-Buandoh, N.G. Mensah, Giant thermoelectric power in fluorine-doped single-walled carbon nanotubes, J. Phys. Chem. Solids. 171 (2022) 111020. https://doi.org/10.1016/j.jpcs.2022.111020.

[29] K.A. Dompreh, K.W. Adu, D. Sakyi-Arthur, N.G. Mensah, S.Y. Mensah, A. Twum, M. Amekpewu, Acoustoelectric current in graphene nanoribbon due to Landau damping, Sci. Rep. 11 (1) (2021) 1–8.

[30] N.R. Sadykov, E.Yu Kocherga, P.N. D'yachkov, Nonlinear current in modified nanotubes with exposure to alternating and constant electric fields, Russ. J. Inorg. Chem. 58 (8) (2013) 951–955.

[31] Michael Mananghaya, Transport properties of ag decorated zigzag graphene nanoribbons as a function of temperature: a density functional based tight binding molecular dynamics study, Adsorption 25 (2019) 1655–1662.

[32] Patrycja Taborowska, Grzegorz Stando, Mika Sahlman, Maciej Krzywiecki, Mari Lundström, Dawid Janas, Doping of carbon nanotubes by halogenated solvents, Sci. Rep. 12 (1) (2022) 1–10.

[33] Bogumiła Kumanek, Tomasz Wasiak, Grzegorz Stando, Paweł Stando, Dariusz Łukowiec, Dawid Janas, Simple method to improve electrical conductivity of films made from single-walled carbon nanotubes, Nanomaterials 9 (8) (2019) 1113.

[34] Bogumiła Kumanek, Grzegorz Stando, Paweł Stando, Karolina Matuszek, Karolina Z. Milowska, Maciej Krzywiecki, Marta Gryglas-Borysiewicz, et al., Enhancing thermoelectric properties of single-walled carbon nanotubes using halide compounds at room temperature and above, Sci. Rep. 11 (1) (2021) 1–18.

[35] J.L. Blackburn, A.J. Ferguson, C. Cho, J.C. Grunlan, Carbon-nanotube-based thermoelectric materials and devices, Adv. Mater. 30 (2018) 1704386, https://doi.org/10.1002/adma.201704386.

[36] J. Ravichandran, Thermoelectric and thermal transport properties of complex oxide thin films, heterostructures and superlattices, J. Mater. Res. 32 (2017) 183–203, https://doi.org/10.1557/jmr.2016.419.

[37] J.S. Bulmer, A. Lekawa-Raus, D.G. Rickel, F.F. Balakirev, K.K. Koziol, Extreme magneto-transport of bulk carbon nanotubes in sorted electronic concentrations and aligned high performance fiber, Sci. Rep. 7 (2017) 12193, https://doi.org/10.1038/s41598-017-12546-6.

[38] D. Janas, Z.K. Milowska, D.P. Bristowe, K.K.K. Koziol, Improving the electrical properties of carbon nanotubes with interhalogen compounds, Nanoscale 9 (2017) 3212–3221, https://doi.org/10.1039/C7NR00224F.